Groundwater Responses to Deluge and Drought in the Fraser Valley, Pacific Northwest

A. H. Nott[1], D. M. Allen[1], and W. J. Hahm[2]

[1]Department of Earth Sciences, Simon Fraser University, Burnaby, BC, Canada. [2]Geography Department, Simon Fraser University, Burnaby, BC, Canada.

Corresponding author: Diana M. Allen (dallen@sfu.ca)

Key Points:

- Two distinct styles of groundwater response to atmospheric rivers and drought occur in coastal valley aquifers
- Meltwater transported via the Fraser River to the coast mediates drought in hydraulically connected aquifers
- Groundwater memory reflects intrinsic aquifer hydraulic properties and encodes the effects of physical boundary conditions

Abstract

Extreme weather events are reshaping hydrological cycles across the globe, yet our understanding of the groundwater response to these extremes remains limited. Here we analyze groundwater levels across the South Coast of British Columbia (BC) in the Pacific Northwest with the objective of determining groundwater responses to atmospheric rivers (ARs) and drought. An AR catalogue was derived and associated to local rainfall defining extreme precipitation. Droughts were quantified using dry day metrics, in conjunction with the standardized precipitation index (SPI). From September to January, approximately 40% of total precipitation is contributed by ARs. From April to September, more than 50% of days receive no precipitation, with typically 26 consecutive dry days. We used the autocorrelation structure of groundwater levels to quantify aquifer memory characteristics and identified two distinct clusters. Cluster 1 wells respond to recharge from local precipitation, primarily rainfall, and respond rapidly to both ARs during winter recharge and significant rainfall deficits during summer. Cluster 2 wells are also driven by local precipitation, and are additionally influenced by the Fraser River's large summer freshet, briefly providing a secondary recharge mechanism to South Coast aquifers. Accordingly, groundwater recessions are offset to later in the summer, contingent on the Fraser River, mediating drought. The results suggest that groundwater memory encapsulates multiple hydrogeological factors, including boundary conditions, influencing the response outcome to extreme events.

Plain Language Summary

Heavy rainfall events and drought are becoming more commonplace around the world. Their effects are immediately observable to us; we see the devastating impacts of floods and the drying of river beds. But we often forget about what happens underground. We sought to shed light on how extremes affect groundwater, the largest accessible freshwater reservoir on Earth. We combined real world observation data on groundwater levels, rainfall, and streamflow within the Pacific Northwest to determine groundwater response to extremes. We found that aquifers connected to large rivers that carry summer snowmelt are more resistant to drought than unconnected aquifers. However, both aquifer groups still depend on heavy rainfall events to recover from drought. As we continue to rely on groundwater for crop irrigation and clean drinking water, climate change will challenge how we manage this resource.

1 Introduction

Anthropogenic climate change will continue to lead to global increases in the intensity, duration, and frequency of extreme weather events (Cook et al., 2022; Dai, 2013; Fowler et al., 2021; Intergovernmental Panel on Climate Change (IPCC), 2023; Kirchmeier-Young & Zhang, 2020; Min et al., 2011; Seneviratne et al., 2012; Zhang et al., 2013; Zhao et al., 2020). These events are reshaping global, regional, and local hydrological cycles and landscapes (Gleeson et al., 2020; Meixner et al., 2016; Peterson et al., 2021; Thomas et al., 2016). Within the terrestrial water cycle, groundwater is the largest accessible freshwater resource reservoir. As such, groundwater is increasingly being relied upon as a source of freshwater (de Graaf et al., 2019; Famiglietti, 2014) for food and water security (Dalin et al., 2019; Taylor et al., 2013), so much so that abstracted groundwater likely accounts for 70% of global irrigation demand (Wood & Cherry,

2021). Yet only 20% of all groundwater on Earth, several hundred metres deep, is actively in flux with the water cycle (Ferguson et al., 2023). Therefore, extreme events disproportionately affect easily accessible shallow groundwater. However, groundwater responses to these extremes remains somewhat unclear.

Extreme precipitation and drought can lead to different responses in groundwater systems depending on the prior series of recharge events and the hydrogeological context (Nygren et al., 2022; Schuler et al., 2022). Mechanistically, recharge is primarily controlled by the antecedent water content, thickness, and infiltration capacity of the vadose zone (de Vries & Simmers, 2002; Fetter & Kreamer, 2021). The vadose zone effectively acts as a reservoir that can store extreme event water (Corona & Ge, 2022), functioning as a recharge signal filter. In many cases, extreme precipitation is an important contributor to groundwater recharge (Corona et al., 2023; Thomas et al., 2016). Unconfined aquifers can respond to infiltration from within several hours to days (Wittenberg et al., 2019), depending on the vadose zone thickness (Schuler et al., 2022). Consistently maintaining a moist vadose zone year-over-year tends to favour groundwater recharge, especially for deeper aquifers (Shao et al., 2018). In temperate climates, Gu et al. (2022) show that total precipitation amounts more strongly influence groundwater levels than event duration. Notwithstanding, events that exceed the infiltration capacity of the vadose zone can trigger overland flow, leading to a reduction in net recharge (Rathay et al., 2018). Reductions in recharge lead to storage depletion, which in turn controls the degree of groundwater drought (Van Loon, 2015).

Drought is a complex and multi-faceted process that can affect—and propagate to—different components of the hydrological cycle (e.g., soil moisture, groundwater, streamflow), contingent on the extent and length of sustained meteorological moisture deficits (Van Lanen, 2006; Van Loon, 2015; W. Wang et al., 2016). During severe droughts, groundwater is usually the last line of defence, maintaining supply to surface water bodies, before ultimately being exhausted (Hellwig et al., 2020). Evapotranspiration (ET) tends to accelerate drought propagation, especially as the atmospheric moisture demand increases (Teuling et al., 2013), increasing temperatures, and establishing a positive feedback loop (Bartusek et al., 2022). While groundwater droughts are primarily driven by precipitation deficits, increases in ET due to anthropogenic warming are likely to become the main driver of groundwater drought (Bloomfield et al., 2019), with the capacity to push hydrologic regimes into new stable states (Peterson et al., 2021).

Groundwater is often considered as possessing a “memory” effect (Brooks et al., 2021; Delbart et al., 2014; Jukić & Denić-Jukić, 2004), because of its ability as a reservoir to store water. Mangin (1984) was among the first to formally quantify the memory characteristics of groundwater, which has been linked to aquifer hydraulic properties (Duy et al., 2021; Van Lanen et al., 2013), the recharge signal (Bloomfield & Marchant, 2013), rates of groundwater discharge (Imagawa et al., 2013), and vadose zone thickness (Schuler et al., 2022). Groundwater memory is being increasingly used as an indicator of aquifer response to drought (Nygren et al., 2022; Schuler et al., 2022; Sutanto & Van Lanen, 2022). The autocorrelation characteristics of groundwater level timeseries attempt to quantify and represent the responsiveness and rate at which external factors (e.g., recharge) are retained by an aquifer, hence the attribution of memory. The theory supposes that a higher memory aquifer will respond more slowly to externals forcings and retain these input signals for longer. Conversely, lower memory aquifers

will respond more quickly and dissipate input signals, leading to a less resilient and more vulnerable aquifer.

In this study, we examine groundwater levels from the Pacific Northwest (PNW), along the South Coast of British Columbia (BC) at the outlet of the Fraser River Basin (FRB). Observation wells are clustered into groups based on the shape of their autocorrelation structure. These clusters are then used to infer recharge mechanisms and memory characteristics. Groundwater responses to ARs and drought are explored by considering the effects of total precipitation, the fraction of AR precipitation, dry days, and consecutive dry days. We hypothesize that aquifer-stream interactions significantly influence aquifer memory characteristics, thereby altering the groundwater response to extremes.

2 Study Area and Methods

2.1 Study Area

The study area is situated in the Pacific Northwest (PNW) and encompasses the Fraser Valley, extending from Hope to the mouth of the Fraser River in the Georgia Strait (Figure 1). The valley is bordered to the north by the Coast Mountains and to the southeast by the Cascade Mountains. An important hydrological feature of the Fraser Valley is the Fraser River, which drains the Fraser River Basin (FRB; inset map in Figure 1) from its Rocky Mountain headwaters, through the Interior Plateau, and down into the Pacific Ocean through the Coast Mountains (Martins et al., 2023). The 1,400 km-long Fraser River is predominantly driven by snow- and glacial melt, with substantial rainfall contribution near the coast, reflecting the collective hydrological input of nearly a third of the province of BC (Déry et al., 2012). Climate across the FRB is diverse with precipitation ranging from 350 mm/yr (<30% as snow) in the Interior Plateau, to about 1000 mm/yr (>50% as snow) in the Rocky Mountains, and over 3000 mm/yr (<15% as snow) in the Coast Mountains (Moore et al., 2010). Snow accumulation typically begins in October, peaks in early April, and melts by early August (Curry & Zwiers, 2018). In contrast, the Fraser Valley features a characteristically temperate ocean climate (Köppen-Geiger: *Cfb* bordering *Csb* (Beck et al., 2018)), receiving on average 1525 mm/yr (range: 1186–1994 mm/yr) of precipitation (1991-2020 climate normals). Snowfall constitutes only 3.3%, or 51 mm/yr (range: 8–200 mm/yr), of precipitation. The mean annual temperature is 10.8 °C, with summer highs around 25 °C, and winter lows just above 0 °C (Figure S1). The Fraser River tends to be event-driven near the coast, where extreme rainfall events can promptly triple the river's discharge (Pawlowicz et al., 2017). The Fraser River can exceed 10,000 m^3/s during freshet peak flows in late June, while low flows (~1,500 m^3/s) persist from December to April (Figure 2b). Peak flows are primarily controlled by the annual maximum snow water equivalent (SWE), and secondarily, by the rate of spring- and summer-time warming (Curry & Zwiers, 2018).

The contemporary physiography of the Fraser Valley is characterized by low relief and flat gently rolling hills (<150 masl) with isolated bedrock outcrops, and bounded by the high relief Coast and Cascade Mountain (Figure 1). This landscape has evolved over hundreds of thousands of years of Quaternary glacial and interglacial processes, largely shaped by the most recent Fraser Glaciation (Clague et al., 1983; Clague & Ward, 2011). Glacio-isostatic adjustment, eustatic sea level change, and successive glacial advances and retreats, have favoured the emplacement of a complex succession of alternating marine, glacial, and non-glacial sediments,

within the Fraser Valley (Armstrong, 1981; Clague, 1994; Clague & James, 2002). Consequently, the spatial distribution and stratigraphy of aquifers and aquitards within the valley can be quite complex. Aquifers, up to 60 m thick, are predominantly sand and gravel of colluvial, fluvial, and glaciofluvial origin (Armstrong, 1984). Aquitards, exceeding 80 m of thickness, are predominantly basal and lodgement tills, and clay and silt of marine, lacustrine, glaciomarine, glaciolacustrine, and glacial origin (Armstrong, 1984).

Groundwater levels in aquifers throughout British Columbia (BC) are monitored by observation wells (OW) through the Provincial Groundwater Observation Well Network (PGOWN) (BC Ministry of Environment and Climate Change Strategy (ECCS), 2023). Figure 1 shows the distribution of OW used in this study. In this study, we broadly classify aquifers as: fractured bedrock, confined sand and gravel (S&G), and unconfined S&G associated with alluvial, glacial outwash or large river systems (Figure 1).

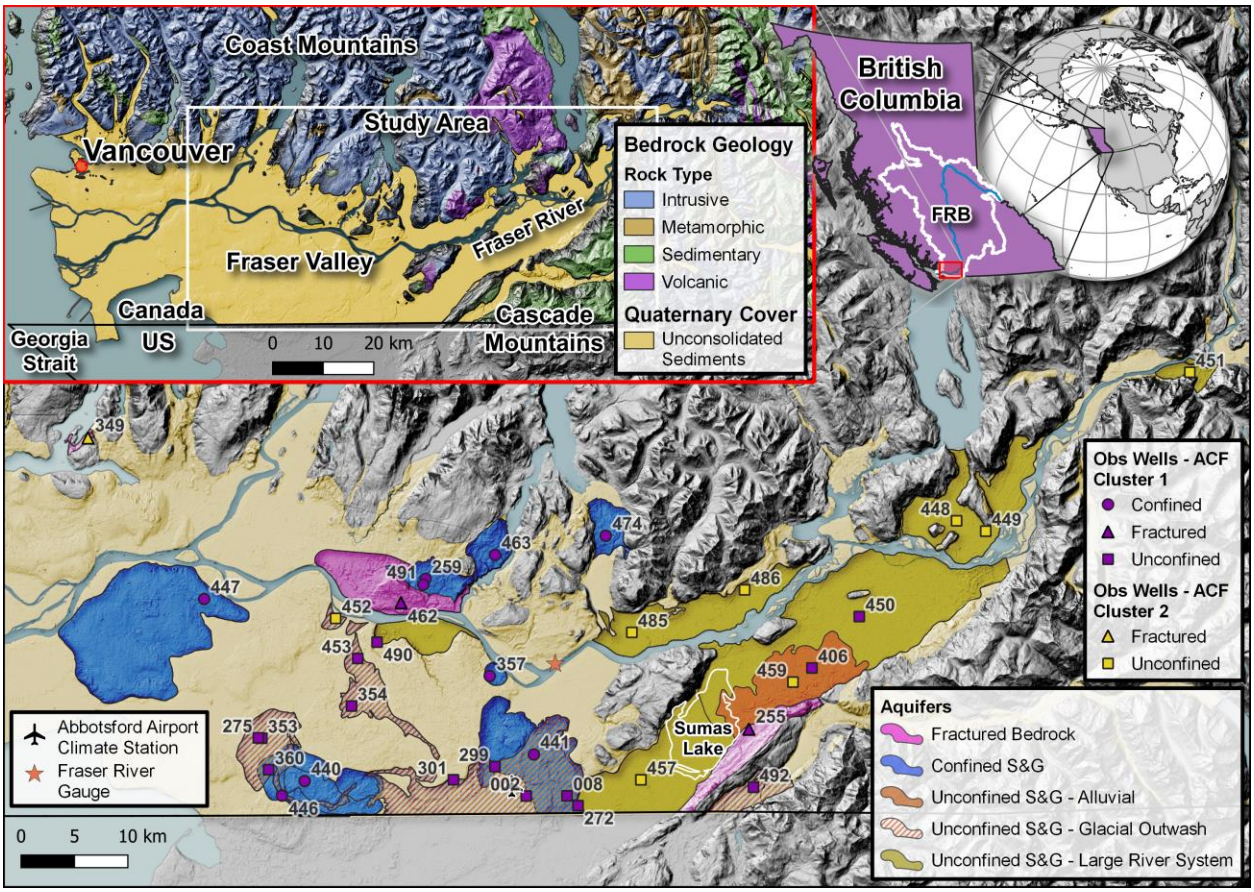

Figure 1. Hydrogeological setting of the Fraser Valley showing the distribution of aquifers (S&G: Sand and Gravel) and provincial observation wells (numbered) along with their associated ACF cluster (see Section 2.5). The Fraser River is the large stream flowing through the valley from east to west. The small provincial inset map shows the Fraser River Basin (FRB) outlined in white with the Fraser River in blue, and the study area is outlined in red. The large inset map shows the underlying bedrock geology (BCGS, 2019) and the extent of unconsolidated

fill deposited during the Quaternary. Map created with QGIS v3.26.3 (QGIS Development Team, 2022).

2.2 Extreme Climate in the Pacific Northwest

Atmospheric Rivers (ARs) are the main mechanism for extreme precipitation events in the PNW (Eldardiry et al., 2019; Sharma & Déry, 2020; Tan et al., 2022) and have been an integral component of Western North America's hydrological cycle for at least 600 years (Borkotoky et al., 2023). ARs are prolonged, extensive, and concentrated bands of enhanced water vapour sourced from tropical or extratropical regions (Neiman et al., 2008; Ralph et al., 2018; Zhu & Newell, 1998). ARs making landfall along the PNW are typically sourced from the northeastern Pacific (20°N–50°N), with mores extremes sourced from the tropics (Nusbaumer & Noone, 2018). While ARs do not always result in extreme precipitation events (Collow et al., 2020), they are important drivers of both flooding and—in their absence—drought persistence (Berghuijs & Slater, 2023; Paltan et al., 2017). The amount of precipitation contributed from landfalling ARs depends heavily on orographic uplift (Ralph et al., 2016; S. Wang et al., 2023), which causes successive depletion in water vapour, controlling the inland penetration (Tan et al., 2022). ARs are important snowpack building events during the winter and at higher altitudes along the North American Cordillera (Eldardiry et al., 2019; Goldenson et al., 2018; Neiman et al., 2008; Paltan et al., 2017; Payne et al., 2020). However, as ARs are transported via warmer moisture circulations, lower elevations can be subject to substantial snowmelt and rain-on-snow events (Chen et al., 2019; Eldardiry et al., 2019; Guan et al., 2016; Spry et al., 2014). In the PNW, higher AR frequency is associated with lower seasonal snowpacks (Goldenson et al., 2018).

In the PNW, drought onset and intensity have increased (Iglesias et al., 2022; Kormos et al., 2016). Moreover, summer baseflow contributions have been in decline (Murray et al., 2023), and likely to deteriorate with continued aridification (Overpeck & Udall, 2020) and increased ET (Liu et al., 2013). Berghuijs et al. (2022) show that climatic aridity imparts a first-order control on whether precipitation recharges groundwater. Notably, the decline in overall precipitation, and winter precipitation arriving as snow, under a warming climate is expected to significantly affect mountain system recharge (Meixner et al., 2016). This is particularly concerning for coastal catchments that oscillate above and below the freezing point both diurnally and seasonally. Coastal groundwater systems relying on snowpack melt for recharge and baseflow supply during summers face heightened risk (Islam et al., 2017; Mote et al., 2005), which is well documented in the mountainous regions of the PNW (Dierauer et al., 2018). Overall, mountainous aquifers are particularly sensitive to region-specific climate and hydrological variables (Gullacher et al., 2023).

The El Niño–Southern Oscillation (ENSO) is the main driver of interannual precipitation variability in the PNW, with less impactful effects from the Pacific Decadal Oscillation (PDO) (Brigode et al., 2013; Fleming & Whitfield, 2010; Lopez & Kirtman, 2019). ENSO can influence extreme precipitation (Brigode et al., 2013) and drought occurrence across the PNW (Vicente-Serrano et al., 2011). During an El Niño, the subtropical jet stream strengthens and shifts equatorward (Payne & Magnusdottir, 2014; Seager et al., 2005), redirecting tropical moisture down into southern California (Young et al., 2017). This causes the PNW to be quite dry and warm during the summer season. Accordingly, these climate teleconnections can significantly influence drought occurrence, and are reflected in the frequency characteristics of groundwater (Malmgren et al., 2022; Rust et al., 2019; Velasco et al., 2017). ARs also tend to be less frequent

during an El Niño summer and winter (Mundhenk et al., 2016). Conversely, the La Niña phase tends to shift storm tracks towards the PNW, increasing winter precipitation (Fleming & Whitfield, 2010) at a time when ARs tend to also be more frequent (Mundhenk et al., 2016; Xiong & Ren, 2021).

2.3 Hydroclimatological Data

AR and integrated vapour transport (IVT) data were obtained from an online catalogue (http://sioftp.ucsd.edu/) maintained by the Center for Western Weather and Water Extremes (CW3E), following the AR detection algorithm described in Rutz et al. (2014). The algorithm constraints for AR detection are: atmospheric water vapour feature length >2000 km and IVT >250 kg m^{-1} s^{-1}. This AR catalogue, as part of the Atmospheric River Tracking Method Intercomparison Project (ARTMIP) (Rutz et al., 2019), identifies the occurrence (or non-occurrence) of landfalling ARs using MERRA-2 gridded climate reanalysis data (Gelaro et al., 2017). AR detection is sensitive to more complex mountainous topography and has been shown to be best resolved by ERA-5 due to a finer spatial resolution (0.25° × 0.25°) (Collow et al., 2022). However, the slightly coarser MERRA-2 (0.5° × 0.625°) AR catalogue was chosen as it was the most up-to-date catalogue (1980–2022). AR data were cropped to an extent of two grid cells (49.0°N, 49.5°N, 121.875°W, 123.125°W) covering the Fraser Valley study region (Figure 1). Then, AR count and mean IVT were converted from three-hourly time steps to daily, if five or more of the eight timesteps were AR occurrences. If an AR was detected in at least one of the grid cells within the study region, then the entire extent was considered to have had an AR occur. This yielded a daily timeseries of AR occurrence and mean IVT. Our derived AR counts in the same region compared well (Figure S2) to both the SIO-R1 AR catalogue by Gershunov et al. (2017) and the distribution of landfalling ARs from CW3E (2022).

Climate data (1980–2022) were obtained from the Abbotsford Airport Climate Station (EC1100030/31) (Figure 2a) operated by Environment and Climate Change Canada (ECCC, 2023) and used to associate precipitation amounts to AR occurrence on any given day. Based on the coarse spatial resolution of the AR catalogue (approx. 45 × 56 km pixels) and the drawbacks of gridded climate data in preserving key features of extreme precipitation (Hu et al., 2018; King et al., 2013; Sun et al., 2018), station-based climate data was deemed appropriate in being able to capture more accurate precipitation associated with ARs.

Given the relatively short record of about two decades for groundwater, we chose to focus on ENSO rather than on the PDO, as the latter tends to highlight interdecadal patterns (15-to-25 years) of climate variability (Mantua & Hare, 2002). The Oceanic Niño Index (ONI) is used to identify the positive (El Niño) and negative (La Niña) phases of ENSO (available from the National Oceanic and Atmospheric Administration's (NOAA) Climate Prediction Center CPC, https://origin.cpc.ncep.noaa.gov/products/analysis_monitoring/ensostuff/ONI_v5.php). The ONI is a three-month running average of sea surface temperature anomalies in the Niño-3.4 region of the Pacific where anomalies above (below) 0.5°C are considered as El Niño (La Niña) events.

2.4 Deluge and Drought Indicators

To investigate the effects of discrete deluge events, first we separated the contribution of AR precipitation to monthly (annual) precipitation by considering the AR fraction of precipitation. The AR fraction was obtained by dividing the total monthly (annual) AR precipitation by the

total monthly (annual) precipitation to isolate any distinct effects ARs might have on groundwater levels.

To quantify discrete drought events, we considered two precipitation-based metrics, consecutive dry day (CDD) and number of dry day (NDD). The CDD fraction was computed by taking the longest run of dry days (precipitation < 1 mm) in a month (year) and dividing by the number of days in a month (year). The NDD fraction is simply a count of dry days (precipitation < 1 mm), divided by the number of days in a month (year).

For determining wet and dry periods, the Standardized Precipitation Index (SPI) (McKee et al., 1993) was computed for precipitation at the Abbotsford Airport Climate Station, using the SCI package (Gudmundsson & Stagge, 2022) in R 4.1.3 (R Core Team, 2022). Several accumulation periods for the SPI were explored (3, 6, 9, 12, and 24), but ultimately, an accumulation period of 6 months was chosen to best represent meteorological drought or deluge at an appropriate temporal scale (Barker et al., 2016). The Pearson type-3 distribution was used for the SPI (see Figure S3, for selection choice). SPI values less (more) than -1 (+1) represent dry (wet) periods (McKee et al., 1993). Therefore, we used the SPI as a metric of classifying wet or dry (meteorological drought) periods, acting as a measure of antecedent wetness or dryness. Linear regression lines are fit between points for SPI less (more) than -1 (+1). This adds more flexibility to exploring groundwater responses in the context of multivariate extremes (Brunner, 2023) over different time scales, where there may be a high CDD or NDD fraction in a positive SPI (wet) period, or conversely, a high AR fraction in a negative SPI (dry) period.

2.5 Hydrogeologic and Hydrometric Data

Streamflow (1965–2022) for the Fraser River at the City of Mission hydrometric station (08MH024) (Figure 2b) was obtained from the Water Survey of Canada (Water Survey of Canada (WSC), 2023). Hourly (upscaled to daily and monthly) groundwater level data for 34 monitoring wells (Figure 2c) were obtained from PGOWN (ECCS, 2023). Care was taken to remove wells with obvious trends or pumping signals; however, there is likely some anthropogenic signal in all monitoring wells. We filtered for well data from 2004 onwards (Figure S4), due to the higher data quality of hourly observations, which prior to, were monthly. Information for 23 aquifers (Table S1) associated to each monitoring well was obtained from the mapped aquifer registry maintained by the BC Ministry of Water, Land and Resource Stewardship (WLRS, 2023). Unfortunately, none of the observation wells have had hydraulic tests performed. Therefore, transmissivity (T) and storativity (S) values were assigned (Table S1) as best estimates (for 26 wells) from various pumping tests conducted around the Fraser Valley (Carmichael, 2013; Cox & Kahle, 1999; Gibbons & Culhane, 1994; Golder Associates Ltd., 2005; Piteau Associates Engineering Ltd., 2012; Ricketts, 1998, 2000; Scibek & Allen, 2005). Fractured aquifer T and S were estimated from literature (Kuang et al., 2020) and well completion reports (ECCS, 2023). We used T, in dimensions of $[L^2/T]$, and S, dimensionless, to determine the hydraulic diffusivity, $D = T/S$, in dimensions of $[L^2/T]$.

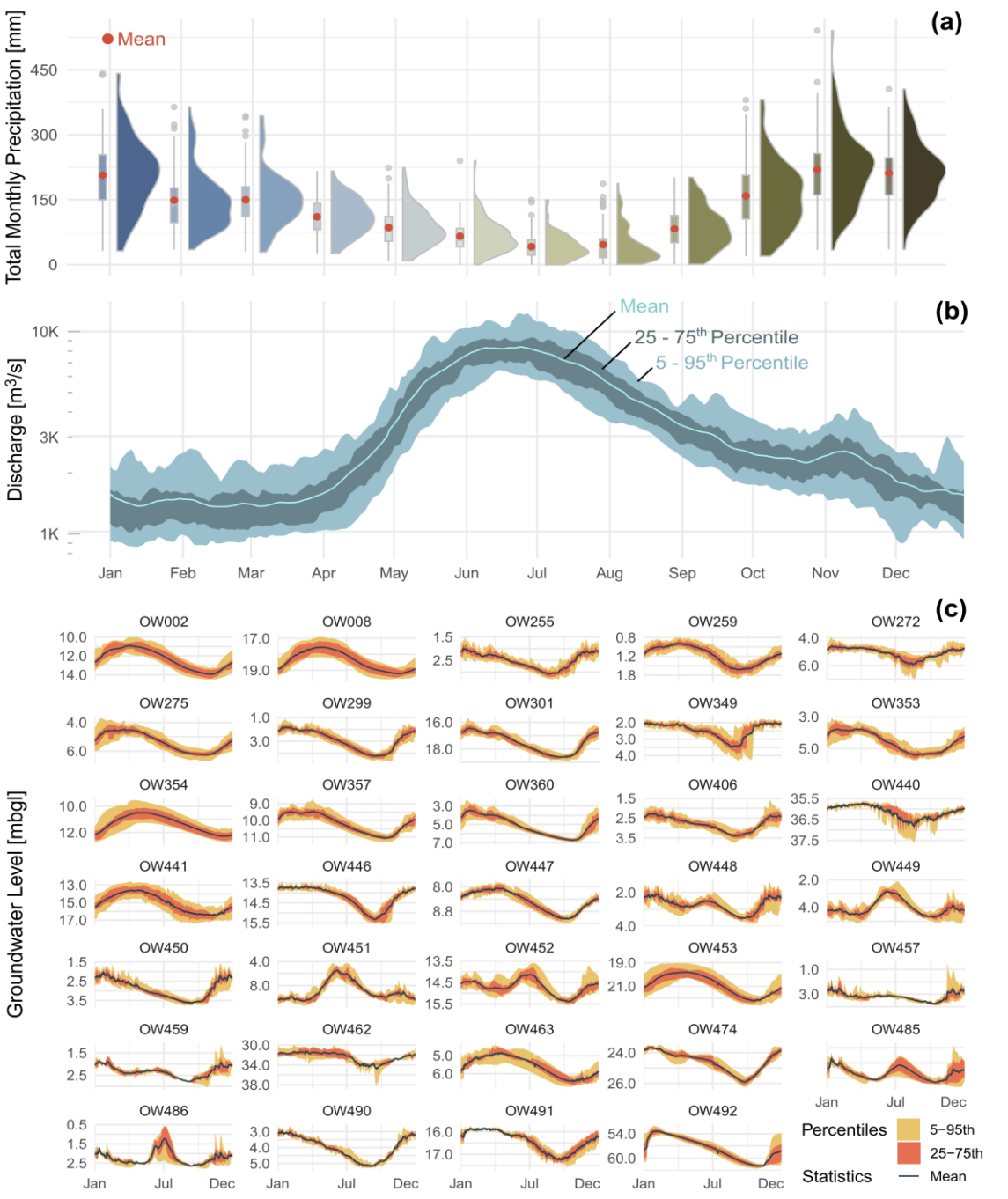

Figure 2. (a) Boxplot and kernel density distributions of monthly precipitation at the Abbotsford Airport Climate Station (EC1100030/31). **(b)** Fraser River discharge at the Mission hydrometric station (08MH024). See Figure 1 for station locations. **(c)** Groundwater level hydrographs.

2.6 Memory Metrics and Autocorrelation Clustering

Autocorrelation measures the linear relationship, or degree of similarity, between subsequent values of the same timeseries lagged over time (Maity, 2018). The autocorrelation function (ACF) of groundwater levels has been widely used in the literature to quantify aquifer memory

in karst and fractured bedrock systems (Bloomfield & Marchant, 2013; Delbart et al., 2016; Lafare et al., 2016; Mangin, 1984; Massei et al., 2006; Schuler et al., 2020), and porous alluvial systems (Duvert et al., 2015; Duy et al., 2021; Imagawa et al., 2013; Nygren et al., 2022; Schuler et al., 2022). The source of this autocorrelation has been linked to autocorrelation in the recharge signal itself, and intrinsic aquifer characteristics (Bloomfield & Marchant, 2013; Duy et al., 2021). Mangin (1984) used an ACF threshold of 0.2 to extract the decorrelation lag time to quantify this memory effect. Massei et al. (2006) emphasized the importance of considering the shape of the ACF in characterizing memory, by fitting a logarithmic function to the ACF at early lag times, to determine a decay rate. This method is often applied to karst systems (Delbart et al., 2016), but has also been used in alluvial systems (Duvert et al., 2015; Duy et al., 2021). Alternatively, a linear fit, to determine decay (slope), can also be applied to early lag times (Delbart et al., 2016; Imagawa et al., 2013).

We used three different ACF-derived metrics to attempt to quantify aquifer memory (Figure 3, summarized in Table S1). First, we considered the traditional decorrelation lag time by threshold (ACF = 0.2). Second, we considered the linear decay rate at early lag times (<150 days) by iteratively fitting a straight line to an optimal fit window of lag times (by maximizing the fit R^2). Finally, we introduce an approach to characterizing the progressive attenuation of the oscillatory ACF pattern. We fit an exponentially decaying (damped) sinusoid function (lag < 1000 days) to determine a decay rate of the ACF oscillation pattern:

$$y(t) = Ae^{-\lambda t}\cos(\omega t - \varphi) \quad (1)$$

where A is the amplitude [-], λ is the exponential decay rate [T^{-1}], ω is the angular frequency [T^{-1}], and φ is the phase shift [-]. See Figures S5, S6, and S7 for the memory metrics mapped to each well.

Exploring memory characteristics revealed distinct ACF shapes (Figure 3). Agglomerative hierarchical clustering, which performs well with groundwater data (Giese et al., 2020; Yin et al., 2022), was applied to groundwater level (GWL) ACFs and optimized two clusters. We applied the Ward Linkage method implementing Euclidean distance as the dissimilarity metric, which tends to result in more distinct and homogenous clusters (Haaf & Barthel, 2018). Clustering was performed using the factoextra R package (Kassambara & Mundt, 2020), and the optimal number of clusters was confirmed using the NbClust R package (Charrad et al., 2014).

2.7 Groundwater Level Adjustments

Groundwater may not immediately respond to ARs or drought. This delay was accounted for by considering a forward lead observation (e.g., considering the following month). Interestingly, GWL rates-of-change (ROC), by successive differencing, cross-correlated with precipitation rate suggest that in nearly all wells, the initial groundwater response can be on the order of days (Figure S8). However, GWL cross-correlated with precipitation reveals that the full response, or total amount of recharge from a precipitation event, is differentially delayed on the order of months (Figure S9). To determine an appropriate lead time adjustment, we checked the cross-correlation lag time (at maximum correlation) between GWLs and precipitation. Lead adjustments range from 2–4 months in confined aquifers, 0–2 months in fractured aquifers, and 0–4 months in unconfined aquifers. Cluster 2 GWLs were unadjusted because of aquifer-stream interactions (discussed below). We assume minimal snow storage acting as lagged recharge based on the snowfall fraction.

2.8 Wavelet Analysis

The Continuous Wavelet Transform (CWT) was used to determine time-averaged frequency spectrums (wavelet spectra) for GWLs, and SPI, using the WaveletComp R package (Roesch & Schmidbauer, 2018). The Wavelet Coherence (WTC) is a measure of coherency (ranging from 0 to 1), or synchronicity in the time-frequency domain, between two signals from the Cross-Wavelet Transform (XWT). The XWT is a time-frequency analogue to cross-correlation, (Torrence & Compo, 1998). The CWT and WTC are advantageous for elucidating changes in frequency over time in non-normal and non-stationary hydrological data (Grinsted et al., 2004; Sang, 2013), and have been effectively applied to groundwater levels (Duvert et al., 2015; Kuss & Gurdak, 2014; Malmgren et al., 2022; Rust et al., 2019). The CWT can be thought of as consecutive band-pass filters (Grinsted et al., 2004) wherein a mother wavelet, here, the Morlet wavelet, is convolved with a timeseries signal. The average wavelet power spectra were min-max normalized to allow for direct comparison between each well, as done in Rust et al. (2019). The time-averaged WTC was used to determine the correlation, in time-frequency space, between GWLs and ENSO (via the ONI), as well as between ENSO and SPI. The significance ($\alpha = 0.05$) of wavelet power, and coherence, were tested via Monte Carlo simulations ($n = 100$), against a null hypothesis that the time series are being driven by a lag-1 autoregressive process (Torrence & Compo, 1998).

3 Results

3.1 Groundwater Clustering and Memory Metrics

Groundwater level responses cluster into one of two groups based on their hydrograph shape (Figure 2), reflected in their autocorrelation structure (Figure 3). Cluster 1 wells are interpreted to respond to recharge from local from precipitation, which is predominantly rainfall within the Fraser Valley. The autocorrelation structure of this cluster oscillates with a periodicity of 365 days (Figure 3a). Some wells display a weak semi-annual signal (Figure 3b, e.g., OW474, 440, 462, 406). The strongest semi-annual signal within cluster 1 is from OW474, which likely reflects a snowmelt contribution to recharge from the adjacent local mountains. The average decorrelation lag time for cluster 1 is about 80 days, but ranges from 65 to 97 days. The linear decay rate, averages -0.012 $days^{-1}$. The dampening of the sinusoidal oscillation of the ACF is represented by he exponential decay rate which can be converted to a half-life. The half-life for cluster 1 is about 954 days. That is, approximately every 3 years, the ACF oscillation amplitude is diminished by half. Overall, cluster 1 wells are a group of relatively high memory aquifers.

Cluster 2 wells not only exhibit a groundwater response that is driven by recharge from local rainfall but are also significantly influenced by the Fraser River due to the strong hydraulic connectivity. Cluster 2 wells are typically low lying and adjacent to the Fraser River (Figure 1), and can be strongly influenced by the Fraser River, which is best observed during the summer freshet (Figure 2). The hydraulic gradient between the Fraser River and OW485 confirms this (Figure S10). During the brief summer freshet, hydraulic gradients are reversed, whereby the Fraser River contributes to adjacent aquifers. For a brief period during the summer, remote, up-catchment mountains in the FRB provide recharge to aquifers in the Fraser Valley. Otherwise, aquifers contribute baseflow to the Fraser River, with gradients reaching their maximum during January (Figure S10). The sole exception is OW349 which has no hydraulic connection to the

Fraser River but mimics its snowmelt response during the summer from the adjacent mountains. While many cluster 1 wells are situated near mountains, snowmelt seems to have little effect on summer groundwater levels.

Cluster 2 wells exhibit an autocorrelation structure that is markedly different than that of cluster 1 wells (Figure 3a), showing twice the ACF oscillation with dual frequency response in annual and semi-annual periodicities (Figure 3b). The additive nature of precipitation seasonality and aquifer-stream interactions with the Fraser River causes this dual signal. The average decorrelation lag time for cluster 2 is about 51 days, but ranges from 40 to 56 days. This average is significantly less than cluster 1 by about 30 days. The linear decay rate at early lag times is about -0.018 days^{-1}. The half-life for cluster 2 is about 392 days, whereby, approximately every year, the ACF oscillation amplitude is diminished by half, dampened much more rapidly than in cluster 1.

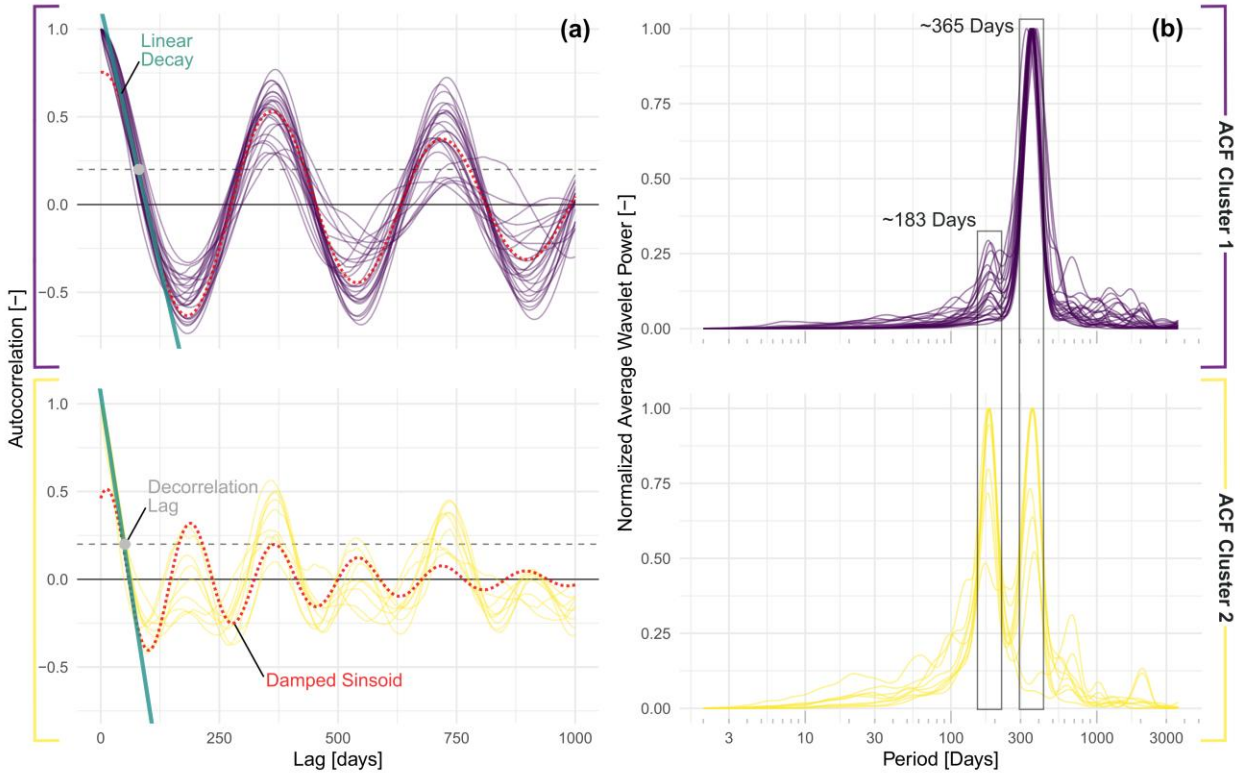

Figure 3. (a) Groundwater ACF clusters and cluster-averaged memory metrics including the linear decay rate, the decorrelation lag time, and the damped sinusoid. **(b)** Frequency characteristics for each ACF cluster based on the normalized average wavelet power.

In determining appropriate groundwater level lead adjustments (see Section 2.6), the cross-correlation between precipitation with GWLs, and GWL ROCs, shed some insight into response times (Table S1). The average GWL-precipitation cross-correlation lag time for confined aquifers (in cluster 1) is 77 days, ranging from 50 to 110 days. Fractured and unconfined aquifers

(in cluster 1) average 58 days, ranging from 2 to 132 days. Cluster 2 wells tend to average 14.3 days, ranging from 2 to 53 days.

3.2 Intra-annual Variability in Deluge and Drought

The majority of ARs make landfall from October to January, but are focused to October and November (Figure 4a), when they are the most intense and likely to result in extreme precipitation events (Figure S11). Expressed as an amount contributed, ARs make up on average more than half of all precipitation received in October (Figure 4b); Gershunov et al. (2017) reported that October to December AR contribution averaged around 50%. Generally, between September and January, ARs contribute around 40% of total precipitation. ARs are generally insignificant contributors to total, or extreme, precipitation during the spring to summer months (Figure 4b), as they are weaker in intensity and carry less moisture (Figure S11).

From April to October, on average, over 50% of the month will receive no precipitation, and over 80% of days in August and July receive no precipitation (Figure 4c). Of those days in August and July, at least two weeks will be continuously dry (Figure 4d). Late summer to early autumn represents a significantly dry and drought-prone period. The transition between significantly dry and significantly wet is relatively rapid; August might be significantly dry but can transition to being significantly wet by October.

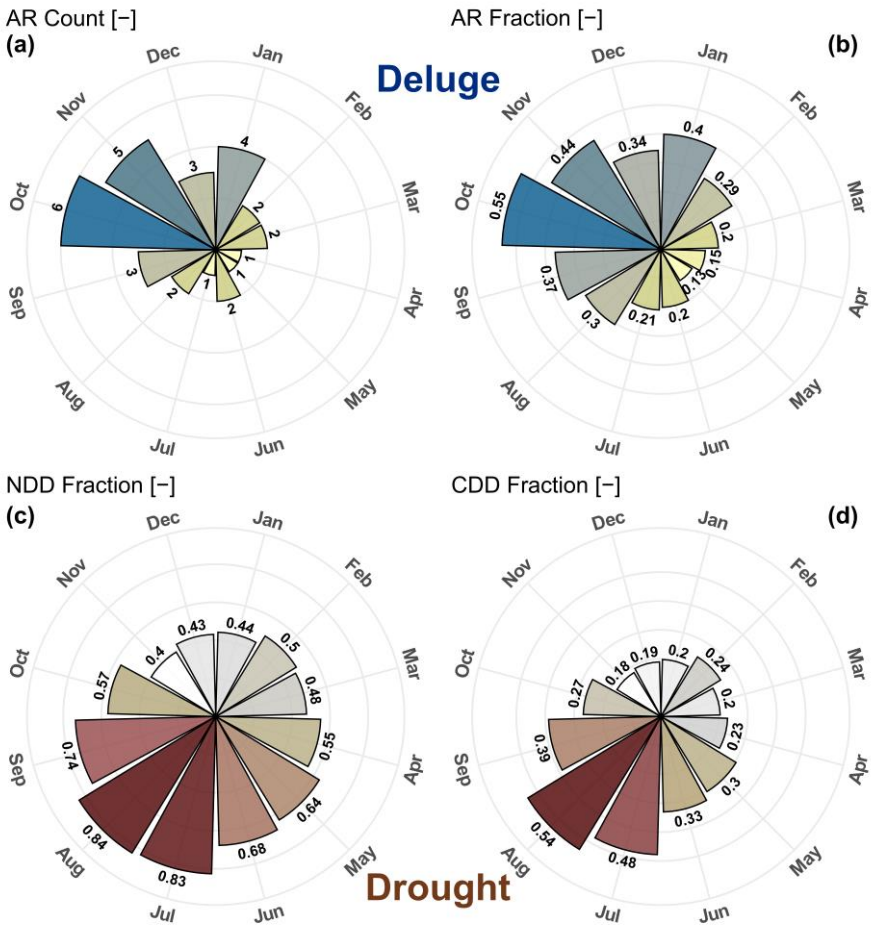

Figure 4. Deluge indicators as monthly averages of AR counts **(a)** and AR fraction of precipitation **(b)**. Drought indicators as average number of dry days (NDD) **(c)** and consecutive dry days (CDD) **(d),** as a fraction of total days in a month.

Monthly groundwater responses reveal a contrast between clusters and their relationship with intra-annual variability in wet and dry periods (Figure 5). GWLs in cluster 1 wells increase as precipitation amounts increase, regardless of SPI (column 1 – Figure 5a). Graphs for all wells are provided in Figure S12. During dry periods (brown) the slope of groundwater levels is steeper, when total precipitation is generally lower. This suggests that aquifers are more responsive to precipitation events during dry periods compared to wet periods. Conversely, during wet periods, the groundwater level response slope is shallower, suggesting that more precipitation does not necessarily result in higher groundwater levels (column 1, Figure 5a). In this case, the infiltration capacity may be reached, as soils are continuously wetted, leading to overland flow and hence, less recharge. For cluster 1 wells, as more precipitation is contributed by ARs (i.e., the AR fraction increases), groundwater levels increase regardless of wet or dry conditions (column 2, Figure 5a). Generally, groundwater level variability in response to higher AR fraction of precipitation is quite high (Figure S13).

Cluster 2 wells tend to show a diverging pattern whereby, during a dry period (negative SPI), the GWL slope is negative (column 1, Figure 5b). During a dry period, as precipitation amounts increase, GWLs seem to decrease. Cluster 2 wells also show a diverging pattern as the AR fraction of precipitation increases (column 2, Figure 5b). AR maximum event intensity follows a similar response; greater intensity ARs are associated with higher groundwater levels, except during dry periods (Figure S14). More intense events are likely to contribute a greater amount to the fraction of precipitation, leading to a greater recharge potential. For example, of the 541 mm of precipitation in November 2021, 153 mm fell in only two days, substantially raising GWLs across the Fraser Valley (Figure 5c). Some cluster 1 wells (e.g., OW406 and OW450 in Figure S13) show a diverging pattern of lower groundwater levels with greater AR fractions of precipitation. We believe this to be a weak influence from the Fraser River, given their relative position to the river (Figure 1), but that the climate signal is stronger, placing them in cluster 1. Overall, this dichotomy between cluster response stresses the adage of correlation versus causation. Greater precipitation does not cause lower groundwater levels. Rather, cluster 2 GWLs are higher in the summer than in early autumn, opposite to cluster 1. This shifts the summer GWL mean to be higher than the autumn mean (Figure 5c), resulting in the diverging patterns observed in Figure 5b.

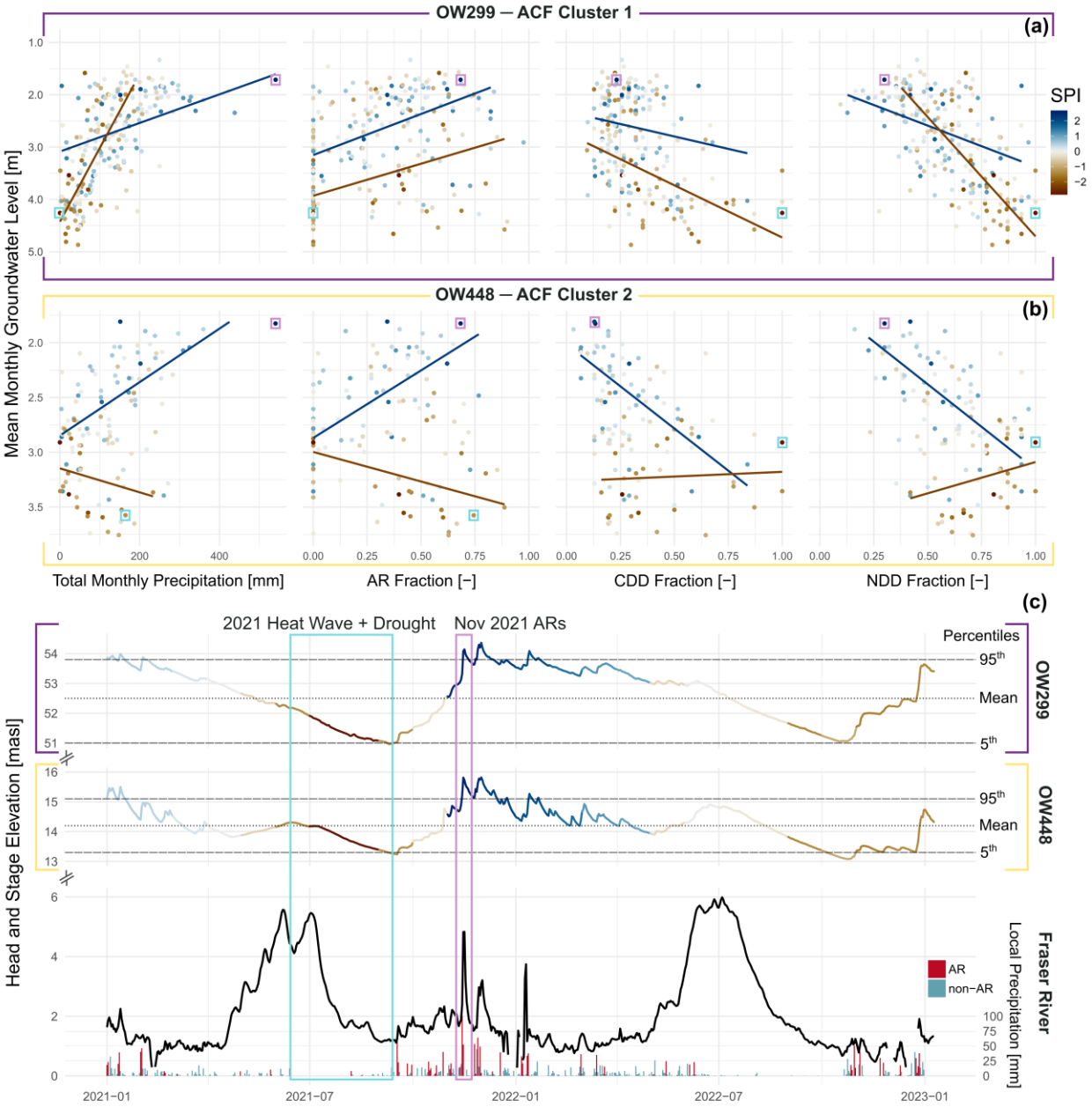

Figure 5. Mean monthly groundwater levels for OW299 **(a)** and OW448 **(b)** as a function of total monthly precipitation, monthly AR fraction, monthly CDD fraction, and monthly NDD fraction. **(c)** Temporal variations in hydraulic heads and stage at Mission (08MH024). The annotated rectangles (teal and purple), mapped in **(a)** and **(b)**, highlight extreme events. Note that the hydrometric station is ~42 km downstream of OW448; therefore, the Fraser River stage is ~10 masl lower than it would be beside OW448.

Longer dry spells (CDD) are associated with lower groundwater levels in both clusters, although cluster 2 wells show a flat response during negative SPI periods (column 3 – Figure 6). CDD fractions less than around 0.5 (two weeks without precipitation) show considerable variations in

groundwater level, regardless of dry or wet periods (Figure S15). A greater NDD is associated with lower GWLs (column 4, Figure 5a); but the dry period response from cluster 2 is opposite (column 4, Figure 5b). The Fraser River freshet coincides with the local climatological dry period of the Fraser Valley, where groundwater levels increase during precipitation deficits (Figure S16). This may not prevent the propagation of drought but can certainly delay its onset. A severe heat wave in June 2021 marked the beginning of significant drought across the Fraser Valley. By mid-July, cluster 2 wells maintained average levels while cluster 1 wells were well below (Figure 5c).

3.3 Inter-annual Variability in Deluge and Drought

The Fraser Valley averages 34 ARs (range: 16–53) per year (1980-2022), contributing to over a third (AR fraction: 37%), or about 571 mm, of total annual precipitation (1542 mm) (Table S2). These results agree with AR studies that include the PNW (Borkotoky et al., 2023; Collow et al., 2022; Gershunov et al., 2017; Tan et al., 2022). Typically, about 60% of the year receives no precipitation, leaving only 40% of the year for potential recharge. Every year averages nearly a full month that receives no precipitation, typically during late summer.

Figure 6b plots the last decade of GWLs for both OW299 (cluster 1) and OW448 (cluster 2), which have similar depths to water table and median GWLs. The interquartile range (IQR) for OW299 is much wider than for OW448, displaying a greater variability in groundwater level throughout a given year. Low GWLs occur around September, while highs are reached around December (Figure 6b).

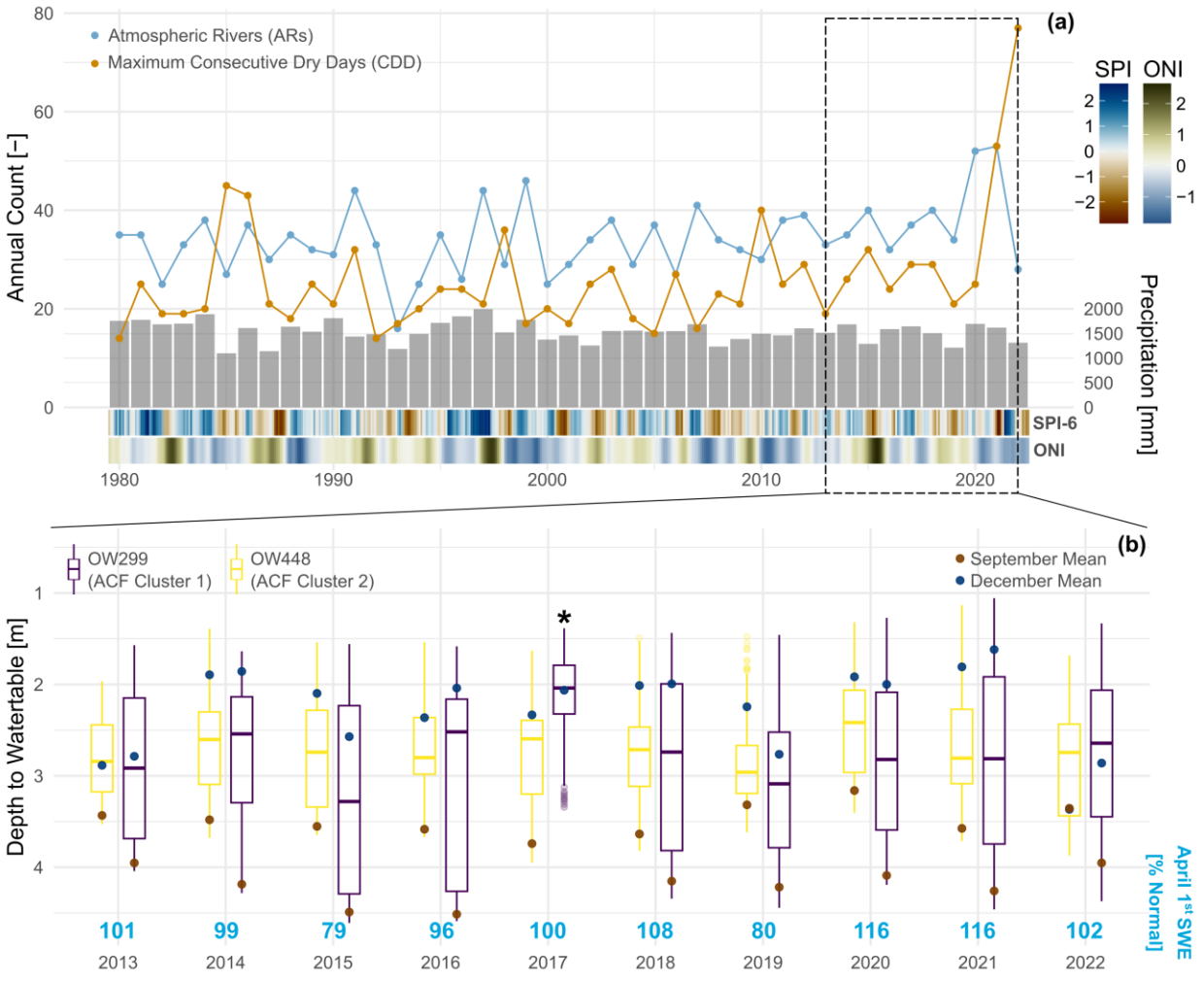

Figure 6. (a) Four decades of hydroclimatology **(b)** Latest decade of water table variations in both clusters as a response to precipitation, ARs, and max CDDs. September (blue) and December (brown) monthly means typify average dry period lows and wet period highs, respectively. April 1st snow water equivalent (SWE) percentage of normal snowpack averaged across the entire FRB is sourced from the BC Snow Survey and Water Supply Bulletin (available from https://www2.gov.bc.ca/gov/content/environment/air-land-water/water/drought-flooding-dikes-dams/river-forecast-centre/snow-survey-water-supply-bulletin). *The 2017 boxplot for OW299 is included for completeness despite missing data from August to November.

Aside from total precipitation, the most influential driver of intra-annual GWL variation seems to be in the timing and distribution of precipitation events. For example, despite an above average snowpack in 2022, nearly three months (end-July to mid-October) without precipitation affected both clusters significantly, resulting in December GWLs well below the annual median (Figure 6b). Warmer winters result in substantially lower snowpacks in the PNW, even if precipitation amounts are within a normal range, as evidenced in 2015 (Mote et al., 2016). Accordingly, cluster 2 wells show lower median groundwater levels during below average snowpack seasons (Figure 6b). These results also support the importance of ARs as significant contributors to

snowpack accumulation, as above average April 1st SWE in 2020 and 2021 were also years that experienced over 50 ARs (Figure 6a). Despite the second highest CDD run in over 40 years, 2021 GWLs across the Fraser Valley were at record highs after receiving 56% of precipitation as ARs (Figure 5c and Table S2).

The cyclicity in dry (SPI < -1) and wet (SPI > 1) periods tends to follow on average a 2-year cycle, with the CWT of SPI-6 (Figure S17) showing a dominant periodicity of 1 to 3 years. Cyclicities in extremes tend correlate more broadly with cycles of ENSO based on the WTC between SPI and ONI, although this is confined to select time periods (Figure S18). SPI and ONI show strong coherence in the 2-year periodicity from 1980 to 1990, 1- to 4-year periodicity from 1998 to 2002, and 3-year periodicity from 2015 to 2020 (Figure S18). This is broadly reflected in interannual GWL variations in the last decade (Figure 6b). Looking at the WTC between GWLs and ENSO cycles, there is significant coherence in the 1- and 2-to-7-year periodicities for cluster 1 wells (Figure S19). The variations in dry-wet periods with ENSO cycles highlights the inter- and intra-annual temporal complexities in climate and weather over the decades: flash droughts can occur during wet winter La Niña (see 2021), while intense ARs can occur dry winter El Niño (see 2015).

4 Discussion

4.1 Groundwater Response to ARs and Drought

Clustering was key in being able to systematically differentiate aquifer responses to extremes, highlighting the complexities of the temporal synchronization of hydrological signals. These signals, and groundwater responses for one representative well from cluster 1 (OW299) and cluster 2 (OW448), are summarized in Figure 7. During winter (1), precipitation (SPI) and the fraction of ARs are both high, while the Fraser River stage (discharge) is low. Both wells have high groundwater levels in response to recharge from autumn and winter precipitation and ARs. Interestingly, Siirila-Woodburn et al. (2023) find that ARs provide less recharge than non-AR precipitation, in a large mountainous catchment in Northern California.

Cluster 2 wells begin to recede earlier, and have much lower GWLs in the spring. During the summer, cluster 1 wells show a decrease in GWLs proportional to decreased precipitation and increased CDDs. Conversely, cluster 2 well GWLs begin to rise, synchronized with the Fraser River, despite precipitation deficits. Both clusters reach a minima in early autumn (2), around October, as precipitation and AR fraction increase. The Fraser River influence on cluster 2 wells is relatively brief, and by early autumn, these wells revert to responding to the availability of diffuse recharge from precipitation, matching cluster 1.

Cluster 2 wells are more drought resilient (to local climate) over nearly the entirety of the summer. The snowpack built up across the FRB can sustain the Fraser River during local meteorological droughts (high fraction of NDD and CDD). However, a low snowpack (snow drought) or a rapid rise in spring temperatures across the FRB generally results in lower summer cluster 2 groundwater levels. Both clusters are particularly sensitive to the number of CDD, which is the main driver for summer and autumn groundwater declines.

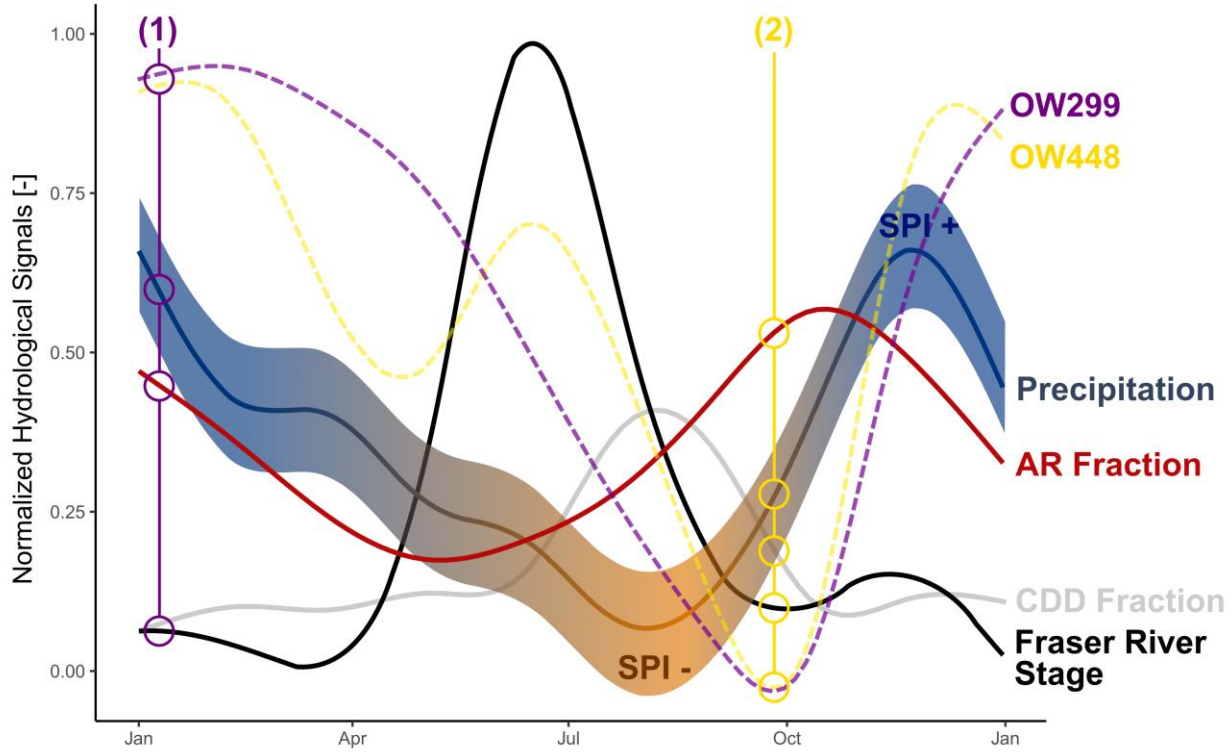

554

555 **Figure 7.** Integrated plot of normalized hydrological signals summarizing the controls of the
556 Fraser River stage, AR fraction of precipitation, CDD fraction, and Precipitation, on the
557 groundwater level response. **(1)** Concurrent periods of high AR precipitation fractions and
558 positive SPI, associated with higher GWLs, present in both clusters. **(2)** GWL minima driven by
559 local climate, in both clusters.

560 4.2 Groundwater Memory Characteristics

561 The decorrelation lag times for porous aquifers ranged from 40 to 97 days, in good agreement
562 with other groundwater studies across the globe. Schuler et al. (2022) report decorrelation lag
563 times between 45 and 154 days in porous aquifers across Ireland, whilst Duy et al. (2021) report
564 values from 35 to 199 days in porous aquifers across the Mekong Delta in Vietnam.

565 While the ACF is an important technique for deriving groundwater memory characteristics, our
566 results suggest broader implications for elucidating the influence of boundary conditions on
567 groundwater response. We show that physical hydrogeological boundaries (aquifer-stream
568 connectivity) can significantly influence the autocorrelation structure of groundwater levels. As
569 expected, the hydraulic properties of an aquifer do not fully explain the variance in ACF-derived
570 memory metrics (Figure 8). To explain why, we focus on the damped decay rate half-life and the
571 decorrelation lag time. The linear decay rate is log-correlated with decorrelation lag time and
572 therefore is redundant (Figure S20).

573 Estimating aquifer hydraulic properties is challenging and often highly uncertain (Kuang et al.,
574 2020), yet is imperative in accurately characterizing groundwater memory. Hydraulic diffusivity,
575 D which acts to dampen hydraulic head responses (H. F. Wang, 2020), integrates T and S into a
576 single property that represents the efficiency in signal propagation. We therefore argue that D is

a fundamental property in governing aquifer memory. Higher diffusivity aquifers have a more rapid GWL recession (Corona et al., 2023), because the response can be propagated more efficiently. Of the wells with hydraulic property data (26), D spans over five orders of magnitude ranging from 0.007 to 260.7 m^2/s. Cluster 2 wells have the greatest D values with a geometric mean of 168.1 m^2/s (range: 101.3–260.7 m^2/s), while cluster 1 wells have a much greater range of D values with a geometric mean of 0.5 m^2/s (range: 0.007–205.9 m^2/s). Generally, a lower D is correlated with higher values of both memory metrics. This relationship is stronger (R^2 = 0.51) when considering D as a function of decorrelation lag time (Figure 8a). While the damped decay rate half-life tends to decrease with decreasing D, the relationship is weaker (R^2 = 0.25) (Figure 8b). As more than half of the total variation in decorrelation lag time is explained by D, this suggests that the damped decay rate half-life reflects a more complex set of factors influencing the ACF.

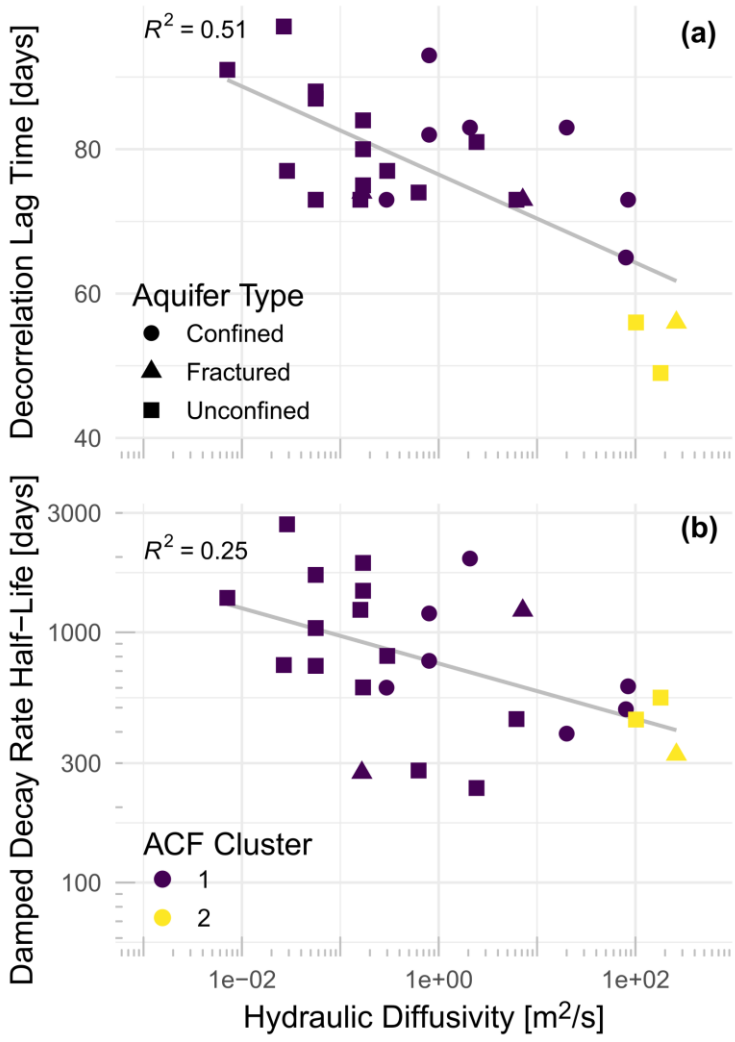

Figure 8. Hydraulic diffusivity as a function of **(a),** the decorrelation lag time, and **(b),** the damped decay rate half-life. Points are colour coded by cluster while point shapes represent the

aquifer type. A linear regression is fit to all points ('lm' function in R) and reported with the coefficient of determination, R^2. Note the log axes.

The disparity in cluster memory metrics raises an important question: do cluster 2 wells really have lower memory than cluster 1 wells? Or would both clusters have similar memory metrics had the Fraser River been absent? We can tease out the answer by observing the relationship between the linear decay rate and the distance of the well to the Fraser River (Figure S21). Cluster 2 wells do tend to be more diffusive by nature of their location and fluvial depositional environment. However, their linear decay rate increases logarithmically with increasing distance away from the Fraser River, approaching cluster 1 decay rates (Figure S21). The linear decay rate for cluster 1 wells seems independent of distance to the Fraser River, despite also including aquifers that are relatively highly diffusive. We posit that cluster 2 wells have lower memory metrics, in part due to higher D, but also because of how effective the Fraser River is at behaving as a boundary condition to groundwater in these aquifers.

4.3 Implications for Groundwater Management

Nearly all Fraser Valley aquifers support agricultural activity, primarily used for irrigation. Peak water use in the South Coast generally occurs from June to September, concomitant with low precipitation. We suggest that cluster 1 wells should be at a higher priority for drought monitoring, as these aquifers respond only to local climate. Groundwater abstraction in cluster 2 wells could be focused during the Fraser River freshet, typically May to June, and minimized closer to the Fraser River autumn minima, in October (Figure 7). Agricultural activities have been linked to increased flood risks because of higher water tables from intense irrigation (Houspanossian et al., 2023). Abstraction during the peak while irrigating during the recession might mitigate this risk. However, during the autumn and winter where ARs can lead to rapid rises in the water table, groundwater flooding is a significant risk. The November 2021 ARs caused widespread flooding (Figure 5c), especially in the old Sumas Lake bed (Figure 1). Unsurprisingly, as cluster 2 associated-aquifers coincide with the Fraser River floodplain, they have been mapped as high flood risk potential (Fraser Basin Council, 2023). Extreme precipitation events in North America, have, and will continue to increase in frequency (Du et al., 2022) and intensity (Li et al., 2019; Prein et al., 2017; Sun et al., 2021). As atmospheric water vapour concentrations increase under continued climate change, ARs at midlatitudes are projected to become stronger and more frequent (Espinoza et al., 2018; S. Wang et al., 2023), especially in the PNW (Gershunov et al., 2019; O'Brien et al., 2022), resulting in less snowfall and more rainfall at mid-elevations (Payne et al., 2020). Presumably, groundwater flooding across the Fraser Valley is likely to become more frequent, especially during late autumn.

The FRB has been shifting from a snow-dominated regime to a hybrid nival-pluvial regime over the past decades (Kang et al., 2014), with future climate warming projected to lead to decreased and earlier peak summer melt (Islam et al., 2019). Climate warming has already begun to affect snow droughts and winter snowpack accumulation across the PNW (Mote et al., 2016). Islam et al. (2017) show that the fraction of precipitation falling as snow across the FRB is projected to significantly decrease, up to 50% by 2050, in addition to an earlier freshet. Although autumn streamflow extremes might be more likely with the projected increase in landfalling ARs across the FRB (Curry et al., 2019).

AR-laden moisture can continue to be transported inland, all the way to central and eastern Canada causing additional rainfall events within 12 days of making landfall on the coast (Vallejo-Bernal et al., 2023). Within a single day of making landfall on the coast, these ARs can contribute significantly to snowpack accumulation in the Rocky Mountains, the headwaters of the Fraser River, even recharging groundwater (Figure S22). However, warming AR circulations have contributed to an overall decrease in AR-related snowfall, even at higher elevations (Sharma & Déry, 2020), which will continue to shift the FRB regime.

5 Conclusions

Extreme events, in both the occurrence and magnitude of ARs and droughts, will continue to increase under a warming climate, shifting groundwater behaviour across the PNW. We analyzed groundwater levels across the Fraser Valley in the South Coast of British Columbia (BC) with the objective of determining groundwater responses to atmospheric rivers (ARs) and drought. On average, 34 ARs make landfall in the Fraser Valley every year, contributing to, on average, 37% of annual precipitation. During peak winter recharge (October to January), around 40% of total precipitation is contributed by ARs, concentrated to October and November. During drought-prone periods (April to September), more than 50% of days receive no precipitation, with typically 26 consecutive dry days. Annual average precipitation, 1542 mm, is concentrated to only about 40% of the year, indicating a concentrated recharge period.

By examining the autocorrelation structure of groundwater levels, a common approach to characterizing aquifer memory, we demonstrated that aquifers in the South Coast region of BC can be influenced by both local and non-local drivers of recharge, mediated by the hydraulic connectivity to the Fraser River. Two distinct clusters are identified using autocorrelation characteristics. Cluster 1 wells respond to recharge from local precipitation, and are quick to respond both ARs during winter recharge season and significant rainfall deficits during the summer. Predictably, cluster 1 groundwater levels increase as the total amount of precipitation or the fraction of AR precipitation increases, regardless of wet or dry season. Similarly, cluster 1 wells respond predictably to dry conditions, with groundwater levels declining with longer dry spells. Cluster 2 wells also respond to recharge from local precipitation during the winter, but are substantially influenced by the Fraser River, which acts as a hydraulic boundary. This hydraulic connectivity between cluster 2 wells and the Fraser River leads to a shift in the timing of groundwater hydrographs relative to local climate conditions. Summer groundwater drought is mediated by the Fraser River's summer freshet, by shifting the recession in cluster 2 wells.

Despite experiencing the same climate, the differentiation in the dominant recharge mechanism (local recharge versus a hydraulic boundary condition) ultimately controls the groundwater response to extremes. Therefore, in this hydrological setting, groundwater memory is controlled by the intrinsic hydraulic properties of an aquifer and encodes the effects of hydraulic boundary conditions. The identification of different drivers of groundwater response can aid in more effective groundwater management strategies in dealing with the effects of climate change, as the hydrological regime of the Fraser River Basin and similar basins across the Pacific Northwest shift from being snow- to rain-dominated.

Acknowledgments

We thank Brian Kawzenuk from the Center for Western Weather and Water Extremes (CW3E) for help accessing the AR catalogue. This project was funded by the Pacific Institute for Climate Solutions (PICS) as a PICS Opportunity Project.

Conflict of Interest

The authors declare no conflicts of interest.

Data Availability Statement

The up-to-date AR catalogue (Rutz et al., (2014) method), used to derive the AR catalogue for the Fraser Valley, is available via file transfer protocol (FTP) at http://sioftp.ucsd.edu/. The derived Fraser Valley AR catalogue, well and aquifer information including memory metrics (Table S1), PGOWN observation well data, and code used in the analysis, are available at http://www.hydroshare.org/resource/d77f11c4ff8245d498faf7b924fe028a. Open data from the government of British Columbia for provincial groundwater observation well data and aquifer information are available from https://catalogue.data.gov.bc.ca/dataset/57c55f10-cf8e-40bb-aae0-2eff311f1685 and https://catalogue.data.gov.bc.ca/dataset/099d69c5-1401-484d-9e19-c121ccb7977c, respectively. Meteorological data for BC are available at https://services.pacificclimate.org/met-data-portal-pcds/app/. Hydrometric data are available at https://wateroffice.ec.gc.ca/search/real_time_e.html.

References

Armstrong, J. E. (1981). *Post-Vashon Wisconsin Glaciation, Fraser Lowland, British Columbia* (Bulletin 322). Geological Survey of Canada. https://doi.org/10.4095/109532

Armstrong, J. E. (1984). *Environmental and Engineering Applications of the Surficial Geology of the Fraser Lowland, British Columbia* (83–23). Geological Survey of Canada. https://doi.org/10.4095/119727

Barker, L. J., Hannaford, J., Chiverton, A., & Svensson, C. (2016). From meteorological to hydrological drought using standardised indicators. *Hydrology and Earth System Sciences*, *20*(6), 2483–2505. https://doi.org/10.5194/hess-20-2483-2016

Bartusek, S., Kornhuber, K., & Ting, M. (2022). 2021 North American heatwave amplified by climate change-driven nonlinear interactions. *Nature Climate Change*, *12*(12), Article 12. https://doi.org/10.1038/s41558-022-01520-4

BCGS. (2019). *Bedrock Geology*. BC Geological Survey. https://catalogue.data.gov.bc.ca/dataset/ef8476ed-b02d-4f5c-b778-0d44c9126144

Beck, H. E., Zimmermann, N. E., McVicar, T. R., Vergopolan, N., Berg, A., & Wood, E. F. (2018). Present and future Köppen-Geiger climate classification maps at 1-km resolution. *Scientific Data*, *5*, 180214. https://doi.org/10.1038/sdata.2018.214

Berghuijs, W. R., Luijendijk, E., Moeck, C., van der Velde, Y., & Allen, S. T. (2022). Global Recharge Data Set Indicates Strengthened Groundwater Connection to Surface Fluxes. *Geophysical Research Letters*, *49*(23), e2022GL099010. https://doi.org/10.1029/2022GL099010

Berghuijs, W. R., & Slater, L. J. (2023). Groundwater shapes North American river floods. *Environmental Research Letters*, *18*(3), 034043. https://doi.org/10.1088/1748-9326/acbecc

Bloomfield, J. P., & Marchant, B. P. (2013). Analysis of groundwater drought building on the standardised precipitation index approach. *Hydrology and Earth System Sciences*, *17*(12), 4769–4787. https://doi.org/10.5194/hess-17-4769-2013

Bloomfield, J. P., Marchant, B. P., & McKenzie, A. A. (2019). Changes in groundwater drought associated with anthropogenic warming. *Hydrology and Earth System Sciences*, *23*(3), 1393–1408. https://doi.org/10.5194/hess-23-1393-2019

Borkotoky, S. S., Williams, A. P., & Steinschneider, S. (2023). Six Hundred Years of Reconstructed Atmospheric River Activity Along the US West Coast. *Journal of Geophysical Research: Atmospheres*, *128*(12), e2022JD038321. https://doi.org/10.1029/2022JD038321

Brigode, P., Mićović, Z., Bernardara, P., Paquet, E., Garavaglia, F., Gailhard, J., & Ribstein, P. (2013). Linking ENSO and heavy rainfall events over coastal British Columbia through a weather pattern classification. *Hydrology and Earth System Sciences*, *17*(4), 1455–1473. https://doi.org/10.5194/hess-17-1455-2013

Brooks, P. D., Gelderloos, A., Wolf, M. A., Jamison, L. R., Strong, C., Solomon, D. K., Bowen, G. J., Burian, S., Tai, X., Arens, S., Briefer, L., Kirkham, T., & Stewart, J. (2021). Groundwater-Mediated Memory of Past Climate Controls Water Yield in Snowmelt-Dominated Catchments. *Water Resources Research*, *57*(10), e2021WR030605. https://doi.org/10.1029/2021WR030605

Brunner, M. I. (2023). Floods and droughts: A multivariate perspective. *Hydrology and Earth System Sciences*, *27*(13), 2479–2497. https://doi.org/10.5194/hess-27-2479-2023

Carmichael, V. (2013). *Compendium of Re-evaluated Pumping Tests in the Regional District of Nanaimo, BC* (p. 941). Ministry of Environment.

https://a100.gov.bc.ca/pub/acat/documents/r36013/RDNPumpingTestReport-Final_1364940347728_26e407c53d6a979b00218722372c4fb2ea7d6c7c60110e4f661734c7bde1889c.pdf

Charrad, M., Ghazzali, N., Boiteau, V., & Niknafs, A. (2014). NbClust: An R Package for Determining the Relevant Number of Clusters in a Data Set. *Journal of Statistical Software*, *61*, 1–36. https://doi.org/10.18637/jss.v061.i06

Chen, X., Leung, L. R., Wigmosta, M., & Richmond, M. (2019). Impact of Atmospheric Rivers on Surface Hydrological Processes in Western U.S. Watersheds. *Journal of Geophysical Research: Atmospheres*, *124*(16), 8896–8916. https://doi.org/10.1029/2019JD030468

Clague, J. J. (1994). *Quaternary stratigraphy and history of south-coastal British Columbia* (481; p. 481). Natural Resources Canada. https://doi.org/10.4095/203249

Clague, J. J., & James, T. S. (2002). History and isostatic effects of the last ice sheet in southern British Columbia. *Quaternary Science Reviews*, *21*(1), 71–87. https://doi.org/10.1016/S0277-3791(01)00070-1

Clague, J. J., Luternauer, J. L., & Hebda, R. J. (1983). Sedimentary environments and postglacial history of the Fraser Delta and lower Fraser Valley, British Columbia. *Canadian Journal of Earth Sciences*, *20*(8), 1314–1326. https://doi.org/10.1139/e83-116

Clague, J. J., & Ward, B. (2011). Chapter 44—Pleistocene Glaciation of British Columbia. In J. Ehlers, P. L. Gibbard, & P. D. Hughes (Eds.), *Developments in Quaternary Sciences* (Vol. 15, pp. 563–573). Elsevier. https://doi.org/10.1016/B978-0-444-53447-7.00044-1

Collow, A. B. M., Mersiovsky, H., & Bosilovich, M. G. (2020). Large-Scale Influences on Atmospheric River–Induced Extreme Precipitation Events along the Coast of Washington State. *Journal of Hydrometeorology*, *21*(9), 2139–2156. https://doi.org/10.1175/JHM-D-19-0272.1

Collow, A. B. M., Shields, C. A., Guan, B., Kim, S., Lora, J. M., McClenny, E. E., Nardi, K., Payne, A., Reid, K., Shearer, E. J., Tomé, R., Wille, J. D., Ramos, A. M., Gorodetskaya, I. V., Leung, L. R., O'Brien, T. A., Ralph, F. M., Rutz, J., Ullrich, P. A., & Wehner, M. (2022). An Overview of ARTMIP's Tier 2 Reanalysis Intercomparison: Uncertainty in the Detection of Atmospheric Rivers and Their Associated Precipitation. *Journal of Geophysical Research: Atmospheres*, *127*(8), e2021JD036155. https://doi.org/10.1029/2021JD036155

765 Cook, B. I., Smerdon, J. E., Cook, E. R., Williams, A. P., Anchukaitis, K. J., Mankin, J. S., Allen, K., Andreu-
766 Hayles, L., Ault, T. R., Belmecheri, S., Coats, S., Coulthard, B., Fosu, B., Grierson, P., Griffin, D., Herrera,
767 D. A., Ionita, M., Lehner, F., Leland, C., … Wise, E. K. (2022). Megadroughts in the Common Era and the
768 Anthropocene. *Nature Reviews Earth & Environment*, *3*(11), Article 11. https://doi.org/10.1038/s43017-
769 022-00329-1
770 Corona, C. R., & Ge, S. (2022). Examining subsurface response to an extreme precipitation event using HYDRUS-
771 1D. *Vadose Zone Journal*, *21*(3), e20189. https://doi.org/10.1002/vzj2.20189
772 Corona, C. R., Ge, S., & Anderson, S. P. (2023). Water-table response to extreme precipitation events. *Journal of*
773 *Hydrology*, *618*, 129140. https://doi.org/10.1016/j.jhydrol.2023.129140
774 Cox, S. E., & Kahle, S. C. (1999). Hydrogeology, ground-water quality, and sources of nitrate in lowland glacial
775 aquifers of Whatcom County, Washington, and British Columbia, Canada. In *Water-Resources*
776 *Investigations Report* (98–4195). U.S. Geological Survey. https://doi.org/10.3133/wri984195
777 Curry, C. L., Islam, S. U., Zwiers, F. W., & Déry, S. J. (2019). Atmospheric Rivers Increase Future Flood Risk in
778 Western Canada's Largest Pacific River. *Geophysical Research Letters*, *46*(3), 1651–1661.
779 https://doi.org/10.1029/2018GL080720
780 Curry, C. L., & Zwiers, F. W. (2018). Examining controls on peak annual streamflow and floods in the Fraser River
781 Basin of British Columbia. *Hydrology and Earth System Sciences*, *22*(4), 2285–2309.
782 https://doi.org/10.5194/hess-22-2285-2018
783 CW3E. (2022, April 7). *Distribution of Landfalling Atmospheric Rivers over the U.S. West Coast During Water*
784 *Year 2022: Summary Through March – Center for Western Weather and Water Extremes*.
785 https://cw3e.ucsd.edu/distribution-of-landfalling-atmospheric-rivers-over-the-u-s-west-coast-during-water-
786 year-2022-summary-through-march/
787 Dai, A. (2013). Increasing drought under global warming in observations and models. *Nature Climate Change*, *3*(1),
788 52–58. https://doi.org/10.1038/nclimate1633
789 Dalin, C., Taniguchi, M., & Green, T. R. (2019). Unsustainable groundwater use for global food production and
790 related international trade. *Global Sustainability*, *2*, e12. https://doi.org/10.1017/sus.2019.7

de Graaf, I. E. M., Gleeson, T., (Rens) van Beek, L. P. H., Sutanudjaja, E. H., & Bierkens, M. F. P. (2019). Environmental flow limits to global groundwater pumping. *Nature*, *574*(7776), Article 7776. https://doi.org/10.1038/s41586-019-1594-4

de Vries, J. J., & Simmers, I. (2002). Groundwater recharge: An overview of processes and challenges. *Hydrogeology Journal*, *10*(1), 5–17. https://doi.org/10.1007/s10040-001-0171-7

Delbart, C., Valdés, D., Barbecot, F., Tognelli, A., & Couchoux, L. (2016). Spatial organization of the impulse response in a karst aquifer. *Journal of Hydrology*, *537*, 18–26. https://doi.org/10.1016/j.jhydrol.2016.03.029

Delbart, C., Valdes, D., Barbecot, F., Tognelli, A., Richon, P., & Couchoux, L. (2014). Temporal variability of karst aquifer response time established by the sliding-windows cross-correlation method. *Journal of Hydrology*, *511*, 580–588. https://doi.org/10.1016/j.jhydrol.2014.02.008

Déry, S. J., Hernández-Henríquez, M. A., Owens, P. N., Parkes, M. W., & Petticrew, E. L. (2012). A century of hydrological variability and trends in the Fraser River Basin. *Environmental Research Letters*, *7*(2), 024019. https://doi.org/10.1088/1748-9326/7/2/024019

Dierauer, J. R., Whitfield, P. H., & Allen, D. M. (2018). Climate Controls on Runoff and Low Flows in Mountain Catchments of Western North America. *Water Resources Research*, *54*(10), 7495–7510. https://doi.org/10.1029/2018WR023087

Du, H., Donat, M. G., Zong, S., Alexander, L. V., Manzanas, R., Kruger, A., Choi, G., Salinger, J., He, H. S., Li, M.-H., Fujibe, F., Nandintsetseg, B., Rehman, S., Abbas, F., Rusticucci, M., Srivastava, A., Zhai, P., Lippmann, T., Yabi, I., … Wu, Z. (2022). Extreme Precipitation on Consecutive Days Occurs More Often in a Warming Climate. *Bulletin of the American Meteorological Society*, *103*(4), E1130–E1145. https://doi.org/10.1175/BAMS-D-21-0140.1

Duvert, C., Jourde, H., Raiber, M., & Cox, M. E. (2015). Correlation and spectral analyses to assess the response of a shallow aquifer to low and high frequency rainfall fluctuations. *Journal of Hydrology*, *527*, 894–907. https://doi.org/10.1016/j.jhydrol.2015.05.054

Duy, N. L., Nguyen, T. V. K., Nguyen, D. V., Tran, A. T., Nguyen, H. T., Heidbüchel, I., Merz, B., & Apel, H. (2021). Groundwater dynamics in the Vietnamese Mekong Delta: Trends, memory effects, and response times. *Journal of Hydrology: Regional Studies*, *33*, 100746. https://doi.org/10.1016/j.ejrh.2020.100746

819 ECCC. (2023). *Abbotsford Airport Climate Station (ID 1100030/1100031)—Environment and Climate Change*
820 *Canada (ECCC)*. PCIC Data Explorer. https://services.pacificclimate.org/met-data-portal-pcds/app/
821 ECCS. (2023). *Provincial Groundwater Observation Well Network (PGOWN)—Ministry of Environment and*
822 *Climate Change Strategy (ECCS)—Groundwater Levels*. https://catalogue.data.gov.bc.ca/dataset/57c55f10-
823 cf8e-40bb-aae0-2eff311f1685
824 Eldardiry, H., Mahmood, A., Chen, X., Hossain, F., Nijssen, B., & Lettenmaier, D. P. (2019). Atmospheric River–
825 Induced Precipitation and Snowpack during the Western United States Cold Season. *Journal of*
826 *Hydrometeorology*, *20*(4), 613–630. https://doi.org/10.1175/JHM-D-18-0228.1
827 Espinoza, V., Waliser, D. E., Guan, B., Lavers, D. A., & Ralph, F. M. (2018). Global Analysis of Climate Change
828 Projection Effects on Atmospheric Rivers. *Geophysical Research Letters*, *45*(9), 4299–4308.
829 https://doi.org/10.1029/2017GL076968
830 Famiglietti, J. S. (2014). The global groundwater crisis. *Nature Climate Change*, *4*(11), 945–948.
831 https://doi.org/10.1038/nclimate2425
832 Ferguson, G., McIntosh, J. C., Jasechko, S., Kim, J.-H., Famiglietti, J. S., & McDonnell, J. J. (2023). Groundwater
833 deeper than 500 m contributes less than 0.1% of global river discharge. *Communications Earth &*
834 *Environment*, *4*(1), Article 1. https://doi.org/10.1038/s43247-023-00697-6
835 Fetter, C. W., & Kreamer, D. (2021). *Applied Hydrogeology: Fifth Edition*. Waveland Press.
836 Fleming, S. W., & Whitfield, P. H. (2010). Spatiotemporal mapping of ENSO and PDO surface meteorological
837 signals in British Columbia, Yukon, and southeast Alaska. *Atmosphere-Ocean*, *48*(2), 122–131.
838 https://doi.org/10.3137/AO1107.2010
839 Fowler, H. J., Lenderink, G., Prein, A. F., Westra, S., Allan, R. P., Ban, N., Barbero, R., Berg, P., Blenkinsop, S.,
840 Do, H. X., Guerreiro, S., Haerter, J. O., Kendon, E. J., Lewis, E., Schaer, C., Sharma, A., Villarini, G.,
841 Wasko, C., & Zhang, X. (2021). Anthropogenic intensification of short-duration rainfall extremes. *Nature*
842 *Reviews Earth & Environment*, *2*(2), 107–122. https://doi.org/10.1038/s43017-020-00128-6
843 Fraser Basin Council. (2023). *Lower Mainland Flood Management Strategy—Synthesis of Technical Analysis*.
844 https://www.fraserbasin.bc.ca/_Library/Water_Flood_Strategy/LMFMS_Synthesis_of_Technical_Analysis
845 _Summer_2023_web.pdf

Gelaro, R., McCarty, W., Suárez, M. J., Todling, R., Molod, A., Takacs, L., Randles, C. A., Darmenov, A., Bosilovich, M. G., Reichle, R., Wargan, K., Coy, L., Cullather, R., Draper, C., Akella, S., Buchard, V., Conaty, A., Silva, A. M. da, Gu, W., … Zhao, B. (2017). The Modern-Era Retrospective Analysis for Research and Applications, Version 2 (MERRA-2). *Journal of Climate*, *30*(14), 5419–5454. https://doi.org/10.1175/JCLI-D-16-0758.1

Gershunov, A., Shulgina, T., Clemesha, R. E. S., Guirguis, K., Pierce, D. W., Dettinger, M. D., Lavers, D. A., Cayan, D. R., Polade, S. D., Kalansky, J., & Ralph, F. M. (2019). Precipitation regime change in Western North America: The role of Atmospheric Rivers. *Scientific Reports*, *9*(1), Article 1. https://doi.org/10.1038/s41598-019-46169-w

Gershunov, A., Shulgina, T., Ralph, F. M., Lavers, D. A., & Rutz, J. J. (2017). Assessing the climate-scale variability of atmospheric rivers affecting western North America. *Geophysical Research Letters*, *44*(15), 7900–7908. https://doi.org/10.1002/2017GL074175

Gibbons, T. D., & Culhane, T. (1994). *Whatcom County Hydraulic Continuity Investigation Part 2: Basin Study of Johnson Creek* (OFTR 94-01). Washington State Department of Ecology. https://www.whatcomcounty.us/DocumentCenter/View/4757/Exhibit-6-PDF?bidId=

Giese, M., Haaf, E., Heudorfer, B., & Barthel, R. (2020). Comparative hydrogeology – reference analysis of groundwater dynamics from neighbouring observation wells. *Hydrological Sciences Journal*, *65*(10), 1685–1706. https://doi.org/10.1080/02626667.2020.1762888

Gleeson, T., Wang-Erlandsson, L., Porkka, M., Zipper, S. C., Jaramillo, F., Gerten, D., Fetzer, I., Cornell, S. E., Piemontese, L., Gordon, L. J., Rockström, J., Oki, T., Sivapalan, M., Wada, Y., Brauman, K. A., Flörke, M., Bierkens, M. F. P., Lehner, B., Keys, P., … Famiglietti, J. S. (2020). Illuminating water cycle modifications and Earth system resilience in the Anthropocene. *Water Resources Research*, *56*(4), e2019WR024957. https://doi.org/10.1029/2019WR024957

Goldenson, N., Leung, L. R., Bitz, C. M., & Blanchard-Wrigglesworth, E. (2018). Influence of Atmospheric Rivers on Mountain Snowpack in the Western United States. *Journal of Climate*, *31*(24), 9921–9940. https://doi.org/10.1175/JCLI-D-18-0268.1

Golder Associates Ltd. (2005). *Comprehensive Groundwater Modelling Assignment: Township of Langley* (022-1826/5000). https://a100.gov.bc.ca/pub/acat/public/viewReport.do?reportId=57709

Grinsted, A., Moore, J. C., & Jevrejeva, S. (2004). Application of the cross wavelet transform and wavelet coherence to geophysical time series. *Nonlinear Processes in Geophysics*, *11*(5/6), 561–566. https://doi.org/10.5194/npg-11-561-2004

Gu, X., Sun, H., Zhang, Y., Zhang, S., & Lu, C. (2022). Partial Wavelet Coherence to Evaluate Scale-dependent Relationships Between Precipitation/Surface Water and Groundwater Levels in a Groundwater System. *Water Resources Management*, *36*(7), 2509–2522. https://doi.org/10.1007/s11269-022-03157-6

Guan, B., Waliser, D. E., Ralph, F. M., Fetzer, E. J., & Neiman, P. J. (2016). Hydrometeorological characteristics of rain-on-snow events associated with atmospheric rivers. *Geophysical Research Letters*, *43*(6), 2964–2973. https://doi.org/10.1002/2016GL067978

Gudmundsson, L., & Stagge, J. H. (2022). *SCI: Standardized Climate Indices Such as SPI, SRI or SPEI* (1.0-2) [Computer software]. https://cran.r-project.org/web/packages/SCI/index.html

Gullacher, A., Allen, D. M., & Goetz, J. D. (2023). Early Warning Indicators of Groundwater Drought in Mountainous Regions. *Water Resources Research*, *59*(8), e2022WR033399. https://doi.org/10.1029/2022WR033399

Haaf, E., & Barthel, R. (2018). An inter-comparison of similarity-based methods for organisation and classification of groundwater hydrographs. *Journal of Hydrology*, *559*, 222–237. https://doi.org/10.1016/j.jhydrol.2018.02.035

Hellwig, J., de Graaf, I. E. M., Weiler, M., & Stahl, K. (2020). Large-Scale Assessment of Delayed Groundwater Responses to Drought. *Water Resources Research*, *56*(2), e2019WR025441. https://doi.org/10.1029/2019WR025441

Houspanossian, J., Giménez, R., Whitworth-Hulse, J. I., Nosetto, M. D., Tych, W., Atkinson, P. M., Rufino, M. C., & Jobbágy, E. G. (2023). Agricultural expansion raises groundwater and increases flooding in the South American plains. *Science*, *380*(6652), 1344–1348. https://doi.org/10.1126/science.add5462

Hu, Z., Zhou, Q., Chen, X., Li, J., Li, Q., Chen, D., Liu, W., & Yin, G. (2018). Evaluation of three global gridded precipitation data sets in central Asia based on rain gauge observations. *International Journal of Climatology*, *38*(9), 3475–3493. https://doi.org/10.1002/joc.5510

Iglesias, V., Travis, W. R., & Balch, J. K. (2022). Recent droughts in the United States are among the fastest-developing of the last seven decades. *Weather and Climate Extremes*, *37*, 100491. https://doi.org/10.1016/j.wace.2022.100491

Imagawa, C., Takeuchi, J., Kawachi, T., Chono, S., & Ishida, K. (2013). Statistical analyses and modeling approaches to hydrodynamic characteristics in alluvial aquifer. *Hydrological Processes*, *27*(26), 4017–4027. https://doi.org/10.1002/hyp.9538

IPCC. (2023). *Climate Change 2021 – The Physical Science Basis: Working Group I Contribution to the Sixth Assessment Report of the Intergovernmental Panel on Climate Change* (1st ed.). Cambridge University Press. https://doi.org/10.1017/9781009157896

Islam, S. U., Curry, C. L., Déry, S. J., & Zwiers, F. W. (2019). Quantifying projected changes in runoff variability and flow regimes of the Fraser River Basin, British Columbia. *Hydrology and Earth System Sciences*, *23*(2), 811–828. https://doi.org/10.5194/hess-23-811-2019

Islam, S. U., Déry, S. J., & Werner, A. T. (2017). Future Climate Change Impacts on Snow and Water Resources of the Fraser River Basin, British Columbia. *Journal of Hydrometeorology*, *18*(2), 473–496. https://doi.org/10.1175/JHM-D-16-0012.1

Jukić, D., & Denić-Jukić, V. (2004). A frequency domain approach to groundwater recharge estimation in karst. *Journal of Hydrology*, *289*(1), 95–110. https://doi.org/10.1016/j.jhydrol.2003.11.005

Kang, D. H., Shi, X., Gao, H., & Déry, S. J. (2014). On the Changing Contribution of Snow to the Hydrology of the Fraser River Basin, Canada. *Journal of Hydrometeorology*, *15*(4), 1344–1365. https://doi.org/10.1175/JHM-D-13-0120.1

Kassambara, A., & Mundt, F. (2020). *factoextra: Extract and Visualize the Results of Multivariate Data Analyses* (R package version 1.0.7) [Computer software]. https://CRAN.R-project.org/package=factoextra

King, A. D., Alexander, L. V., & Donat, M. G. (2013). The efficacy of using gridded data to examine extreme rainfall characteristics: A case study for Australia. *International Journal of Climatology*, *33*(10), 2376–2387. https://doi.org/10.1002/joc.3588

Kirchmeier-Young, M. C., & Zhang, X. (2020). Human influence has intensified extreme precipitation in North America. *Proceedings of the National Academy of Sciences*, *117*(24), 13308–13313. https://doi.org/10.1073/pnas.1921628117

928 Kormos, P. R., Luce, C. H., Wenger, S. J., & Berghuijs, W. R. (2016). Trends and sensitivities of low streamflow
929 extremes to discharge timing and magnitude in Pacific Northwest mountain streams. *Water Resources*
930 *Research*, *52*(7), 4990–5007. https://doi.org/10.1002/2015WR018125
931 Kuang, X., Jiao, J. J., Zheng, C., Cherry, J. A., & Li, H. (2020). A review of specific storage in aquifers. *Journal of*
932 *Hydrology*, *581*, 124383. https://doi.org/10.1016/j.jhydrol.2019.124383
933 Kuss, A. J. M., & Gurdak, J. J. (2014). Groundwater level response in U.S. principal aquifers to ENSO, NAO, PDO,
934 and AMO. *Journal of Hydrology*, *519*, 1939–1952. https://doi.org/10.1016/j.jhydrol.2014.09.069
935 Lafare, A. E. A., Peach, D. W., & Hughes, A. G. (2016). Use of seasonal trend decomposition to understand
936 groundwater behaviour in the Permo-Triassic Sandstone aquifer, Eden Valley, UK. *Hydrogeology Journal*,
937 *24*(1), 141–158. https://doi.org/10.1007/s10040-015-1309-3
938 Li, C., Zwiers, F., Zhang, X., Chen, G., Lu, J., Li, G., Norris, J., Tan, Y., Sun, Y., & Liu, M. (2019). Larger
939 Increases in More Extreme Local Precipitation Events as Climate Warms. *Geophysical Research Letters*,
940 *46*(12), 6885–6891. https://doi.org/10.1029/2019GL082908
941 Liu, M., Adam, J. C., & Hamlet, A. F. (2013). Spatial-temporal variations of evapotranspiration and
942 runoff/precipitation ratios responding to the changing climate in the Pacific Northwest during 1921-2006.
943 *Journal of Geophysical Research: Atmospheres*, *118*(2), 380–394. https://doi.org/10.1029/2012JD018400
944 Lopez, H., & Kirtman, B. P. (2019). ENSO influence over the Pacific North American sector: Uncertainty due to
945 atmospheric internal variability. *Climate Dynamics*, *52*(9), 6149–6172. https://doi.org/10.1007/s00382-018-
946 4500-0
947 Maity, R. (2018). Time Series Analysis. In R. Maity (Ed.), *Statistical Methods in Hydrology and Hydroclimatology*
948 (pp. 305–379). Springer. https://doi.org/10.1007/978-981-10-8779-0_9
949 Malmgren, K. A., C. Neves, M., Gurdak, J. J., Costa, L., & Monteiro, J. P. (2022). Groundwater response to climate
950 variability in Mediterranean type climate zones with comparisons of California (USA) and Portugal.
951 *Hydrogeology Journal*, *30*(3), 767–782. https://doi.org/10.1007/s10040-022-02470-z
952 Mangin, A. (1984). Pour une meilleure connaissance des systèmes hydrologiques à partir des analyses corrélatoire et
953 spectrale. *Journal of Hydrology*, *67*(1), 25–43. https://doi.org/10.1016/0022-1694(84)90230-0
954 Mantua, N. J., & Hare, S. R. (2002). The Pacific Decadal Oscillation. *Journal of Oceanography*, *58*(1), 35–44.
955 https://doi.org/10.1023/A:1015820616384

Martins, E. G., Déry, S. J., & Patterson, D. A. (2023). Chapter 15—Fraser River Basin. In M. D. Delong, T. D. Jardine, A. C. Benke, & C. E. Cushing (Eds.), *Rivers of North America (Second Edition)* (pp. 650–674). Academic Press. https://doi.org/10.1016/B978-0-12-818847-7.00006-9

Massei, N., Dupont, J. P., Mahler, B. J., Laignel, B., Fournier, M., Valdes, D., & Ogier, S. (2006). Investigating transport properties and turbidity dynamics of a karst aquifer using correlation, spectral, and wavelet analyses. *Journal of Hydrology*, *329*(1), 244–257. https://doi.org/10.1016/j.jhydrol.2006.02.021

McKee, T., Doesken, N., & Kleist, J. (1993). *The Relationship of Drought Frequency and Duration to Time Scales*. Eighth Conference on Applied Climatology, Anaheim, California. https://climate.colostate.edu/pdfs/relationshipofdroughtfrequency.pdf

Meixner, T., Manning, A. H., Stonestrom, D. A., Allen, D. M., Ajami, H., Blasch, K. W., Brookfield, A. E., Castro, C. L., Clark, J. F., Gochis, D. J., Flint, A. L., Neff, K. L., Niraula, R., Rodell, M., Scanlon, B. R., Singha, K., & Walvoord, M. A. (2016). Implications of projected climate change for groundwater recharge in the western United States. *Journal of Hydrology*, *534*, 124–138. https://doi.org/10.1016/j.jhydrol.2015.12.027

Min, S.-K., Zhang, X., Zwiers, F. W., & Hegerl, G. C. (2011). Human contribution to more-intense precipitation extremes. *Nature*, *470*(7334), 378–381. https://doi.org/10.1038/nature09763

Moore, R. D., Spittlehouse, D. L., Whitfield, P. H., & Stahl, K. (2010). *Chapter 3—Weather and Climate* (66; Compendium of Forest Hydrology and Geomorphology in British Columbia). Forum for Research and Extension in Natural Resources. https://www.for.gov.bc.ca/hfd/pubs/docs/lmh/Lmh66/LMH66_ch03.pdf

Mote, P. W., Hamlet, A. F., Clark, M. P., & Lettenmaier, D. P. (2005). Declining Mountain Snowpack in Western North America. *Bulletin of the American Meteorological Society*, *86*(1), 39–50. https://doi.org/10.1175/BAMS-86-1-39

Mote, P. W., Rupp, D. E., Li, S., Sharp, D. J., Otto, F., Uhe, P. F., Xiao, M., Lettenmaier, D. P., Cullen, H., & Allen, M. R. (2016). Perspectives on the causes of exceptionally low 2015 snowpack in the western United States. *Geophysical Research Letters*, *43*(20), 10,980-10,988. https://doi.org/10.1002/2016GL069965

Mundhenk, B. D., Barnes, E. A., & Maloney, E. D. (2016). All-Season Climatology and Variability of Atmospheric River Frequencies over the North Pacific. *Journal of Climate*, *29*(13), 4885–4903. https://doi.org/10.1175/JCLI-D-15-0655.1

983 Murray, J., Ayers, J., & Brookfield, A. (2023). The impact of climate change on monthly baseflow trends across
984 Canada. *Journal of Hydrology*, *618*, 129254. https://doi.org/10.1016/j.jhydrol.2023.129254
985 Neiman, P. J., Ralph, F. M., Wick, G. A., Lundquist, J. D., & Dettinger, M. D. (2008). Meteorological
986 Characteristics and Overland Precipitation Impacts of Atmospheric Rivers Affecting the West Coast of
987 North America Based on Eight Years of SSM/I Satellite Observations. *Journal of Hydrometeorology*, *9*(1),
988 22–47. https://doi.org/10.1175/2007JHM855.1
989 Nusbaumer, J., & Noone, D. (2018). Numerical Evaluation of the Modern and Future Origins of Atmospheric River
990 Moisture Over the West Coast of the United States. *Journal of Geophysical Research: Atmospheres*,
991 *123*(12), 6423–6442. https://doi.org/10.1029/2017JD028081
992 Nygren, M., Barthel, R., Allen, D. M., & Giese, M. (2022). Exploring groundwater drought responsiveness in
993 lowland post-glacial environments. *Hydrogeology Journal*, *30*(7), 1937–1961.
994 https://doi.org/10.1007/s10040-022-02521-5
995 O'Brien, T. A., Wehner, M. F., Payne, A. E., Shields, C. A., Rutz, J. J., Leung, L.-R., Ralph, F. M., Collow, A.,
996 Gorodetskaya, I., Guan, B., Lora, J. M., McClenny, E., Nardi, K. M., Ramos, A. M., Tomé, R., Sarangi, C.,
997 Shearer, E. J., Ullrich, P. A., Zarzycki, C., … Zhou, Y. (2022). Increases in Future AR Count and Size:
998 Overview of the ARTMIP Tier 2 CMIP5/6 Experiment. *Journal of Geophysical Research: Atmospheres*,
999 *127*(6), e2021JD036013. https://doi.org/10.1029/2021JD036013
1000 Overpeck, J. T., & Udall, B. (2020). Climate change and the aridification of North America. *Proceedings of the*
1001 *National Academy of Sciences*, *117*(22), 11856–11858. https://doi.org/10.1073/pnas.2006323117
1002 Paltan, H., Waliser, D., Lim, W. H., Guan, B., Yamazaki, D., Pant, R., & Dadson, S. (2017). Global Floods and
1003 Water Availability Driven by Atmospheric Rivers. *Geophysical Research Letters*, *44*(20), 10,387-10,395.
1004 https://doi.org/10.1002/2017GL074882
1005 Pawlowicz, R., Di Costanzo, R., Halverson, M., Devred, E., & Johannessen, S. (2017). Advection, Surface Area,
1006 and Sediment Load of the Fraser River Plume Under Variable Wind and River Forcing. *Atmosphere-*
1007 *Ocean*, *55*(4–5), 293–313. https://doi.org/10.1080/07055900.2017.1389689
1008 Payne, A. E., Demory, M.-E., Leung, L. R., Ramos, A. M., Shields, C. A., Rutz, J. J., Siler, N., Villarini, G., Hall,
1009 A., & Ralph, F. M. (2020). Responses and impacts of atmospheric rivers to climate change. *Nature Reviews*
1010 *Earth & Environment*, *1*(3), 143–157. https://doi.org/10.1038/s43017-020-0030-5

1011 Payne, A. E., & Magnusdottir, G. (2014). Dynamics of Landfalling Atmospheric Rivers over the North Pacific in 30
1012 Years of MERRA Reanalysis. *Journal of Climate*, *27*(18), 7133–7150. https://doi.org/10.1175/JCLI-D-14-
1013 00034.1
1014 Peterson, T. J., Saft, M., Peel, M. C., & John, A. (2021). Watersheds may not recover from drought. *Science*,
1015 *372*(6543), 745–749. https://doi.org/10.1126/science.abd5085
1016 Piteau Associates Engineering Ltd. (2012). *Hydrogeological Investigation For Groundwater Supply: Miracle*
1017 *Valley, B.C.* (Project 3131).
1018 https://www.fvrd.ca/assets/Services/Documents/Water~Systems/FINAL%20REPORT%20FOR%20MIRA
1019 CLE%20VALLEY%20GW%20STUDY%20-%20PITEAU%2004122012%20(FILED).pdf
1020 Prein, A. F., Rasmussen, R. M., Ikeda, K., Liu, C., Clark, M. P., & Holland, G. J. (2017). The future intensification
1021 of hourly precipitation extremes. *Nature Climate Change*, *7*(1), Article 1.
1022 https://doi.org/10.1038/nclimate3168
1023 QGIS Development Team. (2022). *QGIS Geographic Information System* (3.26.3) [Computer software]. QGIS
1024 Association. https://qgis.org/en/site/
1025 R Core Team. (2022). *R: A language and environment for statistical computing* [Computer software]. R Foundation
1026 for Statistical Computing. https://www.R-project.org/
1027 Ralph, F. M., Cordeira, J. M., Neiman, P. J., & Hughes, M. (2016). Landfalling Atmospheric Rivers, the Sierra
1028 Barrier Jet, and Extreme Daily Precipitation in Northern California's Upper Sacramento River Watershed.
1029 *Journal of Hydrometeorology*, *17*(7), 1905–1914. https://doi.org/10.1175/JHM-D-15-0167.1
1030 Ralph, F. M., Dettinger, M. D., Cairns, M. M., Galarneau, T. J., & Eylander, J. (2018). Defining "Atmospheric
1031 River": How the Glossary of Meteorology Helped Resolve a Debate. *Bulletin of the American*
1032 *Meteorological Society*, *99*(4), 837–839. https://doi.org/10.1175/BAMS-D-17-0157.1
1033 Rathay, S. Y., Allen, D. M., & Kirste, D. (2018). Response of a fractured bedrock aquifer to recharge from heavy
1034 rainfall events. *Journal of Hydrology*, *561*, 1048–1062. https://doi.org/10.1016/j.jhydrol.2017.07.042
1035 Ricketts, B. D. (1998). *Groundwater flow beneath the Fraser River delta, British Columbia; a preliminary model*
1036 (Geological Survey of Canada Bulletin 525, pp. 241–255). Geological Survey of Canada.
1037 https://doi.org/10.4095/210047

1038 Ricketts, B. D. (2000). *Modelling of groundwater flow in the Fraser River delta and Brookswood aquifer*
1039 (Geological Survey of Canada Bulletin 552, pp. 103–130). Geological Survey of Canada.
1040 https://doi.org/10.4095/211545
1041 Roesch, A., & Schmidbauer, H. (2018). *WaveletComp: Computational Wavelet Analysis* (R package version 1.1)
1042 [Computer software]. https://CRAN.R-project.org/package=WaveletComp
1043 Rust, W., Holman, I., Bloomfield, J., Cuthbert, M., & Corstanje, R. (2019). Understanding the potential of climate
1044 teleconnections to project future groundwater drought. *Hydrology and Earth System Sciences*, *23*(8), 3233–
1045 3245. https://doi.org/10.5194/hess-23-3233-2019
1046 Rutz, J. J., Shields, C. A., Lora, J. M., Payne, A. E., Guan, B., Ullrich, P., O'Brien, T., Leung, L. R., Ralph, F. M.,
1047 Wehner, M., Brands, S., Collow, A., Goldenson, N., Gorodetskaya, I., Griffith, H., Kashinath, K.,
1048 Kawzenuk, B., Krishnan, H., Kurlin, V., … Viale, M. (2019). The Atmospheric River Tracking Method
1049 Intercomparison Project (ARTMIP): Quantifying Uncertainties in Atmospheric River Climatology. *Journal*
1050 *of Geophysical Research: Atmospheres*, *124*(24), 13777–13802. https://doi.org/10.1029/2019JD030936
1051 Rutz, J. J., Steenburgh, W. J., & Ralph, F. M. (2014). Climatological Characteristics of Atmospheric Rivers and
1052 Their Inland Penetration over the Western United States. *Monthly Weather Review*, *142*(2), 905–921.
1053 https://doi.org/10.1175/MWR-D-13-00168.1
1054 Sang, Y.-F. (2013). A review on the applications of wavelet transform in hydrology time series analysis.
1055 *Atmospheric Research*, *122*, 8–15. https://doi.org/10.1016/j.atmosres.2012.11.003
1056 Scanlon, B. R., Fakhreddine, S., Rateb, A., de Graaf, I., Famiglietti, J., Gleeson, T., Grafton, R. Q., Jobbagy, E.,
1057 Kebede, S., Kolusu, S. R., Konikow, L. F., Long, D., Mekonnen, M., Schmied, H. M., Mukherjee, A.,
1058 MacDonald, A., Reedy, R. C., Shamsudduha, M., Simmons, C. T., … Zheng, C. (2023). Global water
1059 resources and the role of groundwater in a resilient water future. *Nature Reviews Earth & Environment*, 1–
1060 15. https://doi.org/10.1038/s43017-022-00378-6
1061 Schreiner-McGraw, A. P., & Ajami, H. (2021). Delayed response of groundwater to multi-year meteorological
1062 droughts in the absence of anthropogenic management. *Journal of Hydrology*, *603*, 126917.
1063 https://doi.org/10.1016/j.jhydrol.2021.126917

1064 Schuler, P., Campanyà, J., Moe, H., Doherty, D., Williams, N. H., & McCormack, T. (2022). Mapping the
1065 groundwater memory across Ireland: A step towards a groundwater drought susceptibility assessment.
1066 *Journal of Hydrology*, *612*, 128277. https://doi.org/10.1016/j.jhydrol.2022.128277
1067 Schuler, P., Duran, L., Johnston, P., & Gill, L. (2020). Quantifying and Numerically Representing Recharge and
1068 Flow Components in a Karstified Carbonate Aquifer. *Water Resources Research*, *56*(11),
1069 e2020WR027717. https://doi.org/10.1029/2020WR027717
1070 Scibek, J., & Allen, D. M. (2005). *Numerical groundwater flow model of the Abbotsford-Sumas aquifer, central*
1071 *Fraser Lowland of BC, Canada and Washington State, US* (Prepared for Environment Canada). Simon
1072 Fraser University. https://www.sfu.ca/personal/dallen/AB_Modeling_Report_Final.pdf
1073 Seager, R., Harnik, N., Robinson, W. A., Kushnir, Y., Ting, M., Huang, H.-P., & Velez, J. (2005). Mechanisms of
1074 ENSO-forcing of hemispherically symmetric precipitation variability. *Quarterly Journal of the Royal*
1075 *Meteorological Society*, *131*(608), 1501–1527. https://doi.org/10.1256/qj.04.96
1076 Seneviratne, S. I., Nicholls, N., Easterling, D., Goodess, C. M., Kanae, S., Kossin, J., Luo, Y., Marengo, J.,
1077 McInnes, K., Rahimi, M., Reichstein, M., Sorteberg, A., Vera, C., Zhang, X., Rusticucci, M., Semenov, V.,
1078 Alexander, L. V., Allen, S., Benito, G., … Zwiers, F. W. (2012). Changes in Climate Extremes and their
1079 Impacts on the Natural Physical Environment. In C. B. Field, Q. Dahe, T. F. Stocker, & V. Barros (Eds.),
1080 *Managing the Risks of Extreme Events and Disasters to Advance Climate Change Adaptation: Special*
1081 *Report of the Intergovernmental Panel on Climate Change* (pp. 109–230). Cambridge University Press.
1082 https://doi.org/10.1017/CBO9781139177245.006
1083 Seo, K.-W., Ryu, D., Eom, J., Jeon, T., Kim, J.-S., Youm, K., Chen, J., & Wilson, C. R. (2023). Drift of Earth's Pole
1084 Confirms Groundwater Depletion as a Significant Contributor to Global Sea Level Rise 1993–2010.
1085 *Geophysical Research Letters*, *50*(12), e2023GL103509. https://doi.org/10.1029/2023GL103509
1086 Shao, J., Si, B., & Jin, J. (2018). Extreme Precipitation Years and Their Occurrence Frequency Regulate Long-Term
1087 Groundwater Recharge and Transit Time. *Vadose Zone Journal*, *17*(1), 180093.
1088 https://doi.org/10.2136/vzj2018.04.0093
1089 Sharma, A. R., & Déry, S. J. (2020). Contribution of Atmospheric Rivers to Annual, Seasonal, and Extreme
1090 Precipitation Across British Columbia and Southeastern Alaska. *Journal of Geophysical Research:*
1091 *Atmospheres*, *125*(9), e2019JD031823. https://doi.org/10.1029/2019JD031823

1092 Siirila-Woodburn, E. R., Dennedy-Frank, P. J., Rhoades, A., Vahmani, P., Maina, F., Hatchett, B., Zhou, Y., &
1093 Jones, A. (2023). The Role of Atmospheric Rivers on Groundwater: Lessons Learned From an Extreme
1094 Wet Year. *Water Resources Research*, *59*(6), e2022WR033061. https://doi.org/10.1029/2022WR033061
1095 Spry, C. M., Kohfeld, K. E., Allen, D. M., Dunkley, D., & Lertzman, K. (2014). Characterizing Pineapple Express
1096 storms in the Lower Mainland of British Columbia, Canada. *Canadian Water Resources Journal / Revue*
1097 *Canadienne Des Ressources Hydriques*, *39*(3), 302–323. https://doi.org/10.1080/07011784.2014.942574
1098 Sun, Q., Miao, C., Duan, Q., Ashouri, H., Sorooshian, S., & Hsu, K.-L. (2018). A Review of Global Precipitation
1099 Data Sets: Data Sources, Estimation, and Intercomparisons. *Reviews of Geophysics*, *56*(1), 79–107.
1100 https://doi.org/10.1002/2017RG000574
1101 Sun, Q., Zhang, X., Zwiers, F., Westra, S., & Alexander, L. V. (2021). A Global, Continental, and Regional
1102 Analysis of Changes in Extreme Precipitation. *Journal of Climate*, *34*(1), 243–258.
1103 https://doi.org/10.1175/JCLI-D-19-0892.1
1104 Sutanto, S. J., & Van Lanen, H. A. J. (2022). Catchment memory explains hydrological drought forecast
1105 performance. *Scientific Reports*, *12*(1), Article 1. https://doi.org/10.1038/s41598-022-06553-5
1106 Tan, Y., Yang, S., Zwiers, F., Wang, Z., & Sun, Q. (2022). Moisture budget analysis of extreme precipitation
1107 associated with different types of atmospheric rivers over western North America. *Climate Dynamics*,
1108 *58*(3), 793–809. https://doi.org/10.1007/s00382-021-05933-3
1109 Taylor, R. G., Scanlon, B., Döll, P., Rodell, M., van Beek, R., Wada, Y., Longuevergne, L., Leblanc, M.,
1110 Famiglietti, J. S., Edmunds, M., Konikow, L., Green, T. R., Chen, J., Taniguchi, M., Bierkens, M. F. P.,
1111 MacDonald, A., Fan, Y., Maxwell, R. M., Yechieli, Y., … Treidel, H. (2013). Ground water and climate
1112 change. *Nature Climate Change*, *3*(4), 322–329. https://doi.org/10.1038/nclimate1744
1113 Teuling, A. J., Van Loon, A. F., Seneviratne, S. I., Lehner, I., Aubinet, M., Heinesch, B., Bernhofer, C., Grünwald,
1114 T., Prasse, H., & Spank, U. (2013). Evapotranspiration amplifies European summer drought. *Geophysical*
1115 *Research Letters*, *40*(10), 2071–2075. https://doi.org/10.1002/grl.50495
1116 Thomas, B. F., Behrangi, A., & Famiglietti, J. S. (2016). Precipitation Intensity Effects on Groundwater Recharge in
1117 the Southwestern United States. *Water*, *8*(3), Article 3. https://doi.org/10.3390/w8030090

1118 Torrence, C., & Compo, G. P. (1998). A Practical Guide to Wavelet Analysis. *Bulletin of the American*
1119 *Meteorological Society*, *79*(1), 61–78. https://doi.org/10.1175/1520-
1120 0477(1998)079<0061:APGTWA>2.0.CO;2
1121 Vallejo-Bernal, S. M., Wolf, F., Boers, N., Traxl, D., Marwan, N., & Kurths, J. (2023). The role of atmospheric
1122 rivers in the distribution of heavy precipitation events over North America. *Hydrology and Earth System*
1123 *Sciences*, *27*(14), 2645–2660. https://doi.org/10.5194/hess-27-2645-2023
1124 Van Lanen, H. A. J. (2006). Drought propagation through the hydrological cycle. *Climate Variability and Change:*
1125 *Hydrological Impacts*, 122–127.
1126 Van Lanen, H. A. J., Wanders, N., Tallaksen, L. M., & Van Loon, A. F. (2013). Hydrological drought across the
1127 world: Impact of climate and physical catchment structure. *Hydrology and Earth System Sciences*, *17*(5),
1128 1715–1732. https://doi.org/10.5194/hess-17-1715-2013
1129 Van Loon, A. F. (2015). Hydrological drought explained. *WIREs Water*, *2*(4), 359–392.
1130 https://doi.org/10.1002/wat2.1085
1131 Velasco, E. M., Gurdak, J. J., Dickinson, J. E., Ferré, T. P. A., & Corona, C. R. (2017). Interannual to multidecadal
1132 climate forcings on groundwater resources of the U.S. West Coast. *Journal of Hydrology: Regional*
1133 *Studies*, *11*, 250–265. https://doi.org/10.1016/j.ejrh.2015.11.018
1134 Vicente-Serrano, S. M., López-Moreno, J. I., Gimeno, L., Nieto, R., Morán-Tejeda, E., Lorenzo-Lacruz, J.,
1135 Beguería, S., & Azorin-Molina, C. (2011). A multiscalar global evaluation of the impact of ENSO on
1136 droughts. *Journal of Geophysical Research: Atmospheres*, *116*(D20).
1137 https://doi.org/10.1029/2011JD016039
1138 Wang, H. F. (2020). *Groundwater Storage in Confined Aquifers*. The Groundwater Project. https://books.gw-
1139 project.org/groundwater-storage-in-confined-aquifers/
1140 Wang, S., Ma, X., Zhou, S., Wu, L., Wang, H., Tang, Z., Xu, G., Jing, Z., Chen, Z., & Gan, B. (2023). Extreme
1141 atmospheric rivers in a warming climate. *Nature Communications*, *14*(1), Article 1.
1142 https://doi.org/10.1038/s41467-023-38980-x
1143 Wang, W., Ertsen, M. W., Svoboda, M. D., & Hafeez, M. (2016). Propagation of Drought: From Meteorological
1144 Drought to Agricultural and Hydrological Drought. *Advances in Meteorology*, *2016*, 1–5.
1145 https://doi.org/10.1155/2016/6547209

1146 Wittenberg, H., Aksoy, H., & Miegel, K. (2019). Fast response of groundwater to heavy rainfall. *Journal of*
1147 *Hydrology*, *571*, 837–842. https://doi.org/10.1016/j.jhydrol.2019.02.037
1148 WLRS. (2023). *Ground Water Aquifers—Ministry of Water, Land and Resource Stewardship (WLRS)—Aquifer*
1149 *Information*. https://catalogue.data.gov.bc.ca/dataset/099d69c5-1401-484d-9e19-c121ccb7977c
1150 Wood, W. W., & Cherry, J. A. (2021). Food Security and Inaccurate Quantification of Groundwater Irrigation Use.
1151 *Groundwater*, *59*(6), 782–783. https://doi.org/10.1111/gwat.13122
1152 WSC. (2023). *Daily Discharge and Stage for FRASER RIVER AT MISSION (08MH024) [BC]—Water Level and*
1153 *Flow—Environment Canada—Water Survey of Canada*.
1154 https://wateroffice.ec.gc.ca/report/historical_e.html?stn=08MH024
1155 Xiong, Y., & Ren, X. (2021). Influences of Atmospheric Rivers on North Pacific Winter Precipitation: Climatology
1156 and Dependence on ENSO Condition. *Journal of Climate*, *34*(1), 277–292. https://doi.org/10.1175/JCLI-D-
1157 20-0301.1
1158 Yin, J., Medellín-Azuara, J., & Escriva-Bou, A. (2022). Groundwater levels hierarchical clustering and regional
1159 groundwater drought assessment in heavily drafted aquifers. *Hydrology Research*, *53*(7), 1031–1046.
1160 https://doi.org/10.2166/nh.2022.048
1161 Young, A. M., Skelly, K. T., & Cordeira, J. M. (2017). High-impact hydrologic events and atmospheric rivers in
1162 California: An investigation using the NCEI Storm Events Database. *Geophysical Research Letters*, *44*(7),
1163 3393–3401. https://doi.org/10.1002/2017GL073077
1164 Zhang, X., Wan, H., Zwiers, F. W., Hegerl, G. C., & Min, S.-K. (2013). Attributing intensification of precipitation
1165 extremes to human influence. *Geophysical Research Letters*, *40*(19), 5252–5257.
1166 https://doi.org/10.1002/grl.51010
1167 Zhao, C., Brissette, F., Chen, J., & Martel, J.-L. (2020). Frequency change of future extreme summer meteorological
1168 and hydrological droughts over North America. *Journal of Hydrology*, *584*, 124316.
1169 https://doi.org/10.1016/j.jhydrol.2019.124316
1170 Zhu, Y., & Newell, R. E. (1998). A Proposed Algorithm for Moisture Fluxes from Atmospheric Rivers. *Monthly*
1171 *Weather Review*, *126*(3), 725–735. https://doi.org/10.1175/1520-
1172 0493(1998)126<0725:APAFMF>2.0.CO;2
1173